thesis for the degree of Doctor of Philosophy

Coverage Analysis and Beamforming for Dense Cooperative Wireless Networks

Chao Fang

CHALMERS
UNIVERSITY OF TECHNOLOGY

Department of Electrical Engineering
Chalmers University of Technology
Gothenburg, Sweden, 2026

Coverage Analysis and Beamforming for Dense Cooperative Wireless Networks

Chao Fang
ISBN 978-91-8103-446-2

Acknowledgments, dedications, and similar personal statements in this thesis, reflect the author's own views.

Doktorsavhandlingar vid Chalmers tekniska högskola
Ny serie nr 5903
ISSN 0346-718X

Department of Electrical Engineering
Chalmers University of Technology
SE-412 96 Gothenburg, Sweden
Phone: +46 (0)31 772 1000

This work was supported in part by VINNOVA (Swedish Government Agency for Innovation Systems) within the VINN Excellence Centers Chase and ChaseOn, and in part by the European Commission H2020 programme within the 5G PPP mmMAGIC project (grant agreement n°671650). The simulations were performed in part on resources provided by the Swedish National Infrastructure for Computing (SNIC) at C3SE.

Cover: An illustration of densely deployed base stations covering different areas and cooperatively serving user equipment.

Printed by Chalmers Digital Printing
Gothenburg, Sweden, May 2026

To my family

Coverage Analysis and Beamforming for Dense Cooperative Wireless Networks

Chao Fang
Department of Electrical Engineering
Chalmers University of Technology

Abstract

Current and future base stations (BSs) are expected to be densely deployed in places with high traffic demand, such as downtown, stadium, etc., each BS only needs to cover a smaller area compared to current macro BSs. Such network topology can greatly improve the BSs' coverage probability due to the shortened link distance and increased line-of-sight (LoS) transmissions. Moreover, using large spectrum at millimeter-wave (mmWave) frequency bands and highly directional beamforming with large antenna arrays, the network capacity is significantly increased while limiting the interference to other users or BSs.

To model the dense wireless networks where BSs locations follow a random pattern, tools from stochastic geometry are used to express key performance metrics in accurate closed-form equations and to help understand the impact of network design parameters including density, transmit power and number of antennas. Since mmWave systems may be based on novel hybrid beamforming architectures which have reduced hardware power consumption and cost, the beamforming algorithms need to be based on both digital and analog beamforming, novel optimizations in resource allocations and BS cooperation are needed in order to achieve the full potential of mmWave communications, as the signal quality is prone to blockage and high path loss.

In order to provide a better understanding of 5G performance enhancement and limitations, one of the main goals of this thesis is to analyze new models that give tractable performance metrics for dense small BS networks. Another goal in this thesis is to study the resource allocations in multi-cell multi-user mmWave networks and integrated access and backhaul (IAB) networks. In the thesis, we will show the advantages of small cells in improving performance metrics including coverage probability and area spectral efficiency as a result of reduced path loss and shadowing, and we will show the value of cooperation by jointly optimizing the hybrid precoders in mmWave networks and by optimizing the scheduling schemes in IAB networks.

Keywords: Millimeter wave, heterogeneous networks, hybrid beamforming, stochastic geometry, 5G, 6G, beyond 5G, beamforming, integrated access and backhaul (IAB).

List of Publications

This thesis is based on the following publications:

[A] C. Fang, B. Makki, J. Li and T. Svensson, "Hybrid precoding in cooperative millimeter wave networks," *IEEE Trans. Wireless Commun.*, vol. 20, no. 8, pp. 5373-5388, Aug. 2021.

[B] C. Fang, C. Madapatha , B. Makki, and T. Svensson, "Joint scheduling and throughput maximization in self-backhauled millimeter wave cellular networks," *International Symposium on Wireless Communication Systems (ISWCS)*, Berlin, Germany, Sept. 2021, pp. 1-6.

[C] C. Fang, B. Makki, X. Xu and T. Svensson, "Equal gain combining in Poisson networks with spatially correlated interference signals," *IEEE Wireless Commun. Letters*, vol. 5, no. 6, pp. 628-631, Aug. 2016.

[D] C. Fang, B. Makki and T. Svensson, "Coverage analysis for millimeter wave uplink cellular networks with partial zero-forcing receivers," *International Symposium on Modeling and Optimization in Mobile, Ad Hoc, and Wireless Networks (WiOpt)*, Paris, France, May 2017, pp. 1-6.

[E] C. Fang, B. Makki and T. Svensson, "On the performance of the Poisson-point-process-based networks with no channel state information feedback," *IET Communications*, vol. 10, no. 15, pp. 2018-2024, Oct. 2016.

Other publications by the author, not included in this thesis, are:

[F] C. Madapatha, B. Makki, **C. Fang**, O. Teyeb, E. Dahlman, M. Alouini and T. Svensson, "On integrated access and backhaul networks: Current status and potentials," in *IEEE Open Journal of the Communications Society*, vol. 1, pp. 1374-1389, Sept. 2020.

[G] **C. Fang**, B. Makki, J. Li and T. Svensson, "Coordinated hybrid precoding for energy-efficient millimeter wave systems," in *IEEE International Workshop on Signal Processing Advances in Wireless Communications (SPAWC)*, Kalamata, Greece, Jun. 2018, pp. 1-5.

[H] B. Makki, **C. Fang**, T. Svensson, M. Nasiri-Kenari and M. Zorzi, "Delay-sensitive area spectral efficiency: A performance metric for delay-constrained green networks," in *IEEE Trans. Commun.*, vol. 65, no. 6, pp. 2467-2480, Jun. 2017.

[I] X. Chen, **C. Fang**, Y. Zou, A. Wolfgang and T. Svensson, "Beamforming MIMO-OFDM systems in the presence of phase noises at millimeter-Wave frequencies," in *IEEE Wireless Communications and Networking Conference Workshops (WCNCW)*, San Francisco, CA, USA, Mar. 2017, pp. 1-6.

[J] B. Makki, **C. Fang**, T. Svensson, M. Nasiri-Kenari, "On the performance of amplifier-aware dense networks: Finite block-length analysis," in *International Conference on Computing, Networking and Communications (ICNC)*, Kauai, Hawaii, USA, Feb. 2016.

[K] **C. Fang**, B. Makki, Y. Hong, X. Xu, T. Svensson, "HARQ in Poisson point process-based heterogeneous networks," in *Proc. IEEE VTC-Spring*, Glasgow, Scotland, May 2015, pp 1-5.

Acknowledgments

First and foremost, I would like to sincerely thank my main supervisor Prof. Tommy Svensson for offering a PhD position at Chalmers and guide me to expand my knowledge. Your encouragement and constructive feedback have not only improved my understanding of the research but have also contributed to my personal growth. I am grateful for your willingness to go beyond to assist me during the time when I had low motivations and energy. I could not have the achieved milestone without your patience and guidance.

I am also thankful to Dr. Behrooz Makki who has been a great mentor during my research progress. You showed me what it means to do research and your constant feedback has greatly improved my research skills. Thank you for your generosity in sharing your time and knowledge, it has had a significant impact on my academic journey.

Big thanks to all people that I collaborated with during my time at Chalmers. I want to specially express my gratitude to Dr. Jingya Li for her efforts in the discussions, as well as Prof. Xiaodong Xu for his helpful advice in the beginning of my PhD study. Moreover, I want to acknowledge my former colleagues Dr. Yutao Sui, Dr. Hao Guo and Dr. Charitha Madapatha for their support and encouragement.

I would like to thank Prof. Erik Ström and Prof. Fredrik Brännström for the continued efforts in making the CS group attractive and competitive, as well as the administration staff for their assistance. Moreover, special thanks go to everyone in the CS group for making it a great work environment.

Last but not least, I want to express my heartfelt gratitude to my family for being supportive all the time. Special thanks to Suyang, Nana and Milo for bringing so much love and positiveness into my life.

Chao Fang
Stockholm, May 2026

Acronyms

2/3/4/5G:	Second/third/fourth/fifth generation
3GPP:	3rd Generation Partnership Project
ADC:	Analog-to-digital converters
AI:	Artificial intelligence
BS:	Base stations
CCDF:	Complementary cumulative distribution function
CDF:	Cumulative distribution function
CoMP:	Coordinated multi-point
CSI:	Channel state information
DAC:	Digital-to-analog converters
eMBB:	Enhanced mobile broadband
FDP:	Fully digital precoding
FHP:	Fully-connected hybrid precoding
Gbps:	Gigabits per second
HARQ:	Hybrid automatic repeat request
IAB:	Integrated access and backhaul
ITU:	International telecommunication union
LTE:	Long term evolution
LOS:	Line-of-sight
ML:	Machine learning
mmWave:	Millimeter wave
mMTC:	Massive machine type communications
MIMO:	Massive-input massive-output
NLOS:	Non-line-of-sight
PDF:	Probability density function

PHP:	Partially-connected hybrid precoding
PPP:	Poisson point process
PZF:	Partial-zero-forcing
QoS:	Quality-of-service
RF:	Radio frequency
SINR:	Signal-to-interference-plus-noise ratio
SIR:	Signal-to-interference ratio
Tbps:	Terabits per second
URLLC:	Ultra-reliable and low latency communications

Contents

Part I

Overview

CHAPTER 1

Introduction

1.1 Background and Motivation

The shift to a new generation of mobile networks occurs approximately every ten years, this quick evolution of wireless communication technologies has been driven by the lifestyle changes and industry demands. Today, services that require high-resolution video content transmissions and Machine-To-Machine type connections have become a norm. Virtual activities lead to large amount of data transmissions, the viewing time of video streaming is increasing and the applications of connected-home/connected vehicles are also growing fast [1]–[3]. It is clear that 5G with focus on enhanced mobile broadband (eMBB), ultra-reliable and low latency communications (URLLC) and massive machine type communications (mMTC) is the key enabler to meet the demand in the present and near future. Today, around 460 communications service providers have launched 5G services, by the end of 2031, the number of 5G subscriptions is predicted to reach 6.4 billion and around two-thirds of all mobile subscriptions will be 5G [4].

Compared to previous communication networks, 5G greatly enhances the data rate, spectral and energy efficiency, latency, reliability and support for high mobility. According to the minimum performance requirements approved by International Telecommunication Union Radio communication (ITU-R) [5], the downlink peak data rate is 20 Gbps and the peak spectral efficiency is 30 bps/Hz; base stations (BSs) will be able to enter a sleep mode when there is no data to transmit in order to reduce the energy consumption; the user plane latency is down to 4 ms for eMBB and 1 ms for URLLC; BSs are expected to support moving users up to 500 km/h without

interruption time. To meet such performance requirements, the solutions rely on network densification, millimeter wave (mmWave) spectrum with large bandwidth, massive multiple-input-multiple-output (MIMO) antenna arrays, novel beamforming, and coordination[6]–[8].

Network densification is able to fulfill the demand of increasing data rate and coverage by providing traffic hotspots with short range. Small cells, e.g., femtocells, can be deployed in locations that are closer to users in order to facilitate line-of-sight (LOS) transmissions and reduce the competition for resource blocks and outage zones [9]. Clearly, 5G networks will be heterogeneous with BSs of different hardware configurations, cell range and backhaul methods [10], [11]. Developing accurate and tractable models for heterogeneous networks has drawn considerable attention [12]–[20]. Due to the small cells' arbitrary locations, modeling the locations of the BSs by stochastic geometry has been shown to achieve as accurate result as the popular grid model, and it allows simple expressions to be derived for the signal-to-interference-plus-noise ratio (SINR) distribution.

The widely-discussed challenges for network densification are interference coordination and cell association[10], [21]–[23]. Depending on the deployment, network densification may cause interference to small-cell users in the uplink or cell-edge macro-cell users in the downlink. Interference coordination in dense networks including orthogonal transmissions, optimal scheduling, power control, and frequency reuse is particularly important for reducing unexpected and strong interference, specially if the network is not well planned. Cell association is another key challenge for dense networks, as it is optimal for users to be associated to the BSs with maximum SINR and less traffic load [24]–[26]. Due to the variety of cell sizes and the large numbers of the BSs, pushing users to small cells requires additional overhead and coordination. Furthermore, for moving users, handovers involving small BSs presents some unique challenges [27], [28]. Last but not least, small BSs need backhauling through either fiber or wireless links, which puts requirements on the capacity, cost and flexibility of backhaul links [29]–[31]. Most research works assume small cells are connected to the core network with fixed fiber links, and it may not be practical due to the large number of distributed small cells. Hence, wireless backhaul solutions should be further investigated to enhance the performance of dense networks.

As one of the novel features, 5G is characterized by the use of mmWave spectrum. Due to the fact that the spectrum below 6 GHz used by previous communication systems is fully occupied, mmWave communications are able to achieve high data rate by using large spectrum in the mmWave bands. The main reason why mmWave spectrum was previously considered unsuitable for mobile communications is the high path loss, rain and atmospheric absorption which greatly limit the transmission range, and also because high bandwidths of mmWave bands were not really required in the previous generations of wireless networks. Today, technologies such as mmWave low-cost CMOS circuitry and high-gain miniaturized antennas have made mmWave more

practical than before [7]. The small wavelength allows building high gain antenna arrays on a small-scale chip, which will help counter the higher propagation loss associated with high frequency signals. Among the challenges related to mmWave communications, channel modeling and beamforming architectures are of particular importance.

Having an accurate channel model is essential for studying and testing mmWave communication solutions. In the recent years, there has been an increasing amount of measurement and simulation data on mmWave channel modeling, results of path loss exponent, delay spreads and angular spread have been studied at mmWave frequencies and different scenarios [32]–[38]. Based on the measurement results, channel models are mainly developed from the 3GPP 3D channel model or geometry-based stochastic model [39]. The most important channel modeling requirements include improving the spatial accuracy regarding path and sub-path modeling, supporting very large bandwidth and considering blocking and scattering objects.

Since large antenna arrays are employed in 5G BSs, the conventional digital beamforming architecture which requires a complete radio-frequency (RF) chain for each antenna may be too costly and complex. Most research concerning mmWave beamforming schemes have adopted alternative architectures including hybrid architecture [40]–[44], switch based architecture [45]–[47] and low-precision analog-to-digital converters (ADCs) [48]–[50]. In a single cell setup, it has been shown that these alternative architectures can achieve high data rate close to that of the fully digital architecture by optimizing beamforming precoders and combiners. Hence, one of the main requirements for mmWave beamforming architecture is that power consumption, cost and complexity should be kept as low as possible while maintaining a high spectral efficiency.

For multi-cell and multi-user setups, the joint user selection and coordinated multipoint (CoMP) transmissions between BSs is a candidate technology to achieve high spectrum efficiency and make the network robust to the change of channel conditions. Many researchers have proposed cooperative beamforming methods in mmWave networks [51]–[54]. Hybrid beamforming is studied in cell-free MIMO scenarios considering access point power constraints [51]. In [52], the user-beam selection problem, where the BSs jointly select directional beams and users in order to maximize the users' rates, is studied. Considering multiple cells and pre-associated users, hybrid precoding methods maximizing the per-user SINR are proposed in [53]. The achievable rate of coordinated beamforming achieved by using deep learning to predict the beamforming vectors is shown in [54]. However, many of the CoMP schemes, including the full coordination among BSs that allows multiple streams transmitting jointly from multiple BSs, need further study. They should align with mmWave systems characteristics including the number of RF chains, the number of streams and the number of clusters in the channel [55].

5G backhaul networks will likely be upgraded to include integrated access and

backhaul (IAB) technology, possibly operating at mmWave frequencies, and providing high capacity and flexibility [30], [56]–[62]. Traditional backhaul methods mainly rely on fiber links or fixed wireless links. While fiber provides reliable links with high peak rate, fiber installation may lead to high installation/maintenance cost, and trenching/infrastructure displacement. Also, fiber installation may not be allowed in, e.g., historical areas. Wireless backhaul, on the other hand, comes with high flexibility and easy installation, at the cost of low peak rate. Traditional wireless backhaul techniques are mainly based on non-standardized solutions with LOS links operating in 10-80 GHz. With 5G, however, the access links will operate in the mmWave frequency, i.e., the range which was previously used for backhaul. Also, with small cells, there is a need to support non-line-of-sight (NLOS) backhaul. These two are the main motivations for the IAB networks, as specified in 3GPP 5G NR. Considering multi-hop transmission and a large number of BSs and users, scheduling and resource allocations have been studied to achieve high throughput and energy efficiency [63]–[66]. However, the study on IAB networks incorporating mmWave channel characteristics and advanced antenna techniques have not been much exploited and needs further investigations [67].

While 5G is becoming a reality and constantly evolving, the discussion about 6G has already started [68]–[74]. As 5G unfolds and emerging applications are becoming mature, 6G will be mainly driven by the advancement of high-fidelity holographic society, connectivity for all things, and time sensitive applications. Still the key performance indicators and the requirements of 6G are not determined, while there are predictions of the 6G quality-of-service (QoS) requirements and new use cases such as integrated Sensing and Communication that greatly improve signal quality; In order to provide high quality multimedia services to a large number of users, 6G may need to provide peak data rate up to 1 Terabits per second (Tbps) in some specific use-cases, compared to 20 gigabits per second (Gbps) in 5G. To meet the demand of delay-sensitive applications such as tactile internet, 6G may target user experienced latency less than 10 ms. In order to support extreme reliability, e.g., remote surgery, the error rate may need to reach 10^{-6} in 6G, which is 100 times smaller than that in 5G. In addition, 6G aims to support even larger coverage, denser users and higher mobility than that of 5G. Also, as a key feature, 6G is expected to broadly utilize artificial intelligence/machine learning, which helps in increasing the autonomous functionality of the network, at the cost of, e.g., uplink traffic increment. Although applications and requirements of 6G put significant challenges on the development of 5G, 5G is still evolving and is ready to meet the demand of our society in the next decade. The standards and enabling technologies of 6G will be truly revealed as we proceed the research beyond 5G.

1.2 Aim of Thesis

The aim of the thesis is to provide performance analysis on heterogeneous and mmWave communication systems with dense BS deployments and BS cooperation. Performance metrics including coverage probability and area spectral efficiency are analysed in Poisson point process (PPP) based networks where analytical expressions are derived in closed form. Considering BS cooperation, energy-efficient hybrid precoding algorithms are proposed to enable BS joint transmissions and achieve users' QoS requirements. Furthermore, in IAB networks, where BSs can transmit and receive backhaul data using the access channels, a joint access and backhaul link scheduling algorithm is proposed to maximize the minimum throughput in the cases with multiple users.

The analytical study of the thesis is useful in improving the network performance in the following aspects:

- Enabling scalable analysis and simulations in dense networks with a large number of BSs and users.
- Understanding the impact of key design parameters including BS density, number of antennas, transmit and interference power on the coverage-related metrics in dense networks.
- Considering the impact of different hybrid precoding architectures, hardware power consumption is included in the analysis to achieve high energy and spectral efficiency.
- Providing joint hybrid precoding schemes and demonstrating the benefits of BS cooperation, such as reducing network outage probability and RF transmit power variation.
- Providing joint scheduling algorithms to analyse the throughput performance of IAB networks with different types of BSs and multiple backhaul hops.

1.3 Organization of Thesis

The thesis is divided into two parts. Part I gives an introduction to Part II where a collection of papers are included. The remainder of Part I is organized as follows. In Chapter 2, we introduce different methods for modeling dense networks. In Chapter 3, beamforming architectures in mmWave cellular systems are given and a brief introduction to optimization techniques in CoMP networks is provided. Chapter 4 introduces the IAB concept. Finally, Chapter 5 summarizes the contributions in the appended papers.

1.4 Notation

We use bold lower-case letters like $\mathbf{d}$ for vectors and upper-case bold letters like $\mathbf{R}$ for matrices. $\mathbf{R}^T$, $\mathbf{R}^H$, $\mathbf{R}^{(i,j)}$ and $||\mathbf{R}||_F$ denote the transpose, the Hermitian, the (i,j)-th entry of $\mathbf{R}$ and the Frobenius norm of $\mathbf{R}$, respectively. $\mathbb{C}^n$ represents the set of n-tuples of complex numbers represented as column vectors and $\mathbb{C}^{m\times n}$ denotes the set of complex $m \times n$ matrices. $\mathbb{E}$ and $\mathbb{V}$ denote the expectation and variance operators.

CHAPTER 2

Network Densification

In this chapter, we discuss the advantages and challenges of network desification. As illustrated in Fig. 2.1, a macro cell is densified by adding small cells to offload the traffic from the macro BS and reduce the service outage area. Because small cells are usually deployed closer to the users, such as on lamp posts or on the side of walls, the received signal strength is in general improved due to the reduced path loss and increased LOS probability. However, increasing cell density requires careful interference management, if the deployment is not well planned. If a user is connected to a macro BS, nearby small BSs may cause significant interference if they transmit in the same time-frequency block. Therefore, along with network planning, interference management techniques such as CoMP and advanced multi-antenna transmissions can further increase the capacity that network densification can provide.

As small cells have different transmit powers, coverage area and hardware, compared to macro BSs, in dense metropolitan areas, 5G networks tend to be heterogeneous and the locations of small cells may be distributed in a less regular pattern. In order to obtain tractable performance metrics in a network with a large number of cells, stochastic geometry, which has been shown to be a useful tool in characterizing such networks [15], [75], [76], enables tractable results in terms of SINR distributions.

2.1 Heterogeneous Cellular Networks

Heterogeneous cellular networks is typically described as consisting of K spatially and spectrally coexisting tiers, where each tier is distinguished by its transmit power, BS

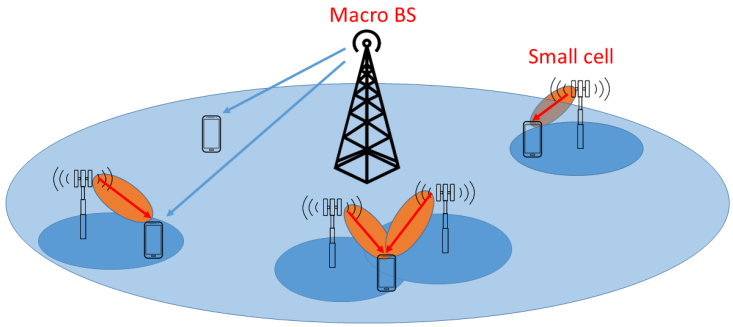

Figure 2.1: A heterogeneous network with a macro cell and densely deployed small cells. Users can be served by one or multiple BSs.

density, and data rate. For example, macro cells (tier 1) would typically have much higher transmit power and lower density than the higher tiers (e.g., small cells). Small cells may have unstructured locations and provide users with high data rate in a short range, while macro cells can maintain communication links in a long range.

Increasing small cell density may also result in increased inter-cell interference. Moreover, since path loss, small-scale fading and interference are all dependent on the locations of the BSs, taking the spatial randomness of the BSs into consideration when modeling networks has attracted considerable attention. For this reason, stochastic geometry, where the BSs are modeled as one or several point process(es), is more suitable to analyze the performance of heterogeneous networks than conventional models [77], [78]. The reason is that the statistical performance metrics can be obtained in tractable forms and the small cells topology resembles a realization of random point process.

2.2 Stochastic Geometry

In order to better understand how to model wireless networks using stochastic geometry, we give an introduction to mathematical tools in stochastic geometry and discuss simple applications of modeling wireless networks. Figure 2.2 shows the actual locations of the BSs in a central part of Stockholm, Sweden. We notice that the structure of the BSs forms a less regular pattern, thus, it is sensible to model wireless networks with randomness in the BS spatial distributions. In particular, stochastic geometry analyzes the performance of wireless networks averaged over a large number of realizations rather than a specific network configuration, which lets

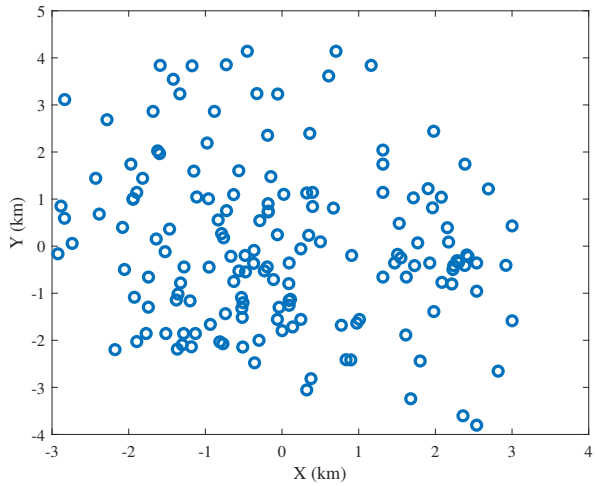

Figure 2.2: Actual BS locations in central Stockholm, Sweden. The data contains mainly the LTE and GSM BSs and shows a highly dense and unstructured network topology.

us predict the performance for an ensemble of wireless networks.

Point process, which studies points randomly located in a space, is considered as the main sub-field of stochastic geometry. The simplest and widely-used point process in modeling wireless networks is PPP. A point process Φ is Poisson on a space E if, for all sets A of E, the points $\Phi(A)$ are independently located in A and the random variables $\Phi(A)$ are Poisson distributed [79]. PPP has the following properties which make certain network metrics easy-to-compute:

- A PPP is homogeneous, if the density of the points is constant across the plane.
- A PPP is stationary, if the law of the point process is invariant to translation.
- A PPP is simple, if two points can not take the same location.
- The superposition of two independent PPPs is still a PPP.
- The independent thinning of a PPP, in which certain points are removed from the PPP, is still a PPP.

The intensity of a PPP $\lambda(x)$ is a function of the location, while for homogeneous PPP the intensity is a constant λ. For many operations on PPP, we can compute the new intensity in closed-form. PPP may be transformed by mapping each point of the process to another point. Let f be a function $\mathbb{R}^d \rightarrow \mathbb{R}^s$, then

$$\Phi' = f(\Phi) = \cup_{x \in \Phi} f(x), \tag{2.1}$$

is a PPP with intensity measure

$$\Lambda'(A') = \Lambda(f^{-1}(A')) = \int_{f^{-1}(A')} \lambda(x)\mathrm{d}x, \quad \text{for all sets } A' \in \mathbb{R}^s. \tag{2.2}$$

When a stationary PPP is independently thinned by deleting each point with probability $1-g(x)$, the thinning process generates an inhomogeneous PPP with intensity $\lambda g(x)$. In wireless networks, the point process of current active transmitters is a thinned version of the point process considering all nodes.

Many theorems related to PPP are useful for modeling wireless networks. Slivnyak's Theorem [80, Theorem 8.10] states that the law of a PPP conditioned on a point at a given location is the same as the law of a PPP without that point. The theorem allows us to model the transmitters with PPP and, considering a receiver at the origin, the properties of the PPP do not change whether or not we condition on the receiver. Campbell's Theorem [80, Theorem 4.1] is another handy property for PPP. It states that, if Φ has an intensity $\lambda(x)$ and $S = \sum_{x\in\Phi} f(x)$ is a random sum where $f : \mathbb{R}^d \to \mathbb{R}$, then

$$\mathbb{E}(S) = \int_{\mathbb{R}^d} f(x)\lambda(x)\mathrm{d}x, \tag{2.3}$$

and

$$\mathbb{V}(S) = \int_{\mathbb{R}^d} f^2(x)\lambda(x)\mathrm{d}x, \tag{2.4}$$

where $\mathbb{E}$ and $\mathbb{V}$ denote the expectation and variance operators, respectively. Equations (2.3) and (2.4) are useful when calculating the mean and the variance of the interference in a network, as we can model the total interference at a receiver as the sum power from all other interfering transmitters. For more properties of the PPP and point processes, where nodes are clustered or separated, see [80], [81].

2.3 Interference Analysis

Consider a receiver y and a set of active transmitters $\Phi = \{x_i\}$ that are distributed in a 2-dimensional plane according to homogeneous PPP with density λ, for single antenna systems, the interference power at y is given by

$$I(y) = \sum_{x_i\in\Phi} P|h_{x_i}|^2 \ell\left(||x_i - y||\right), \tag{2.5}$$

where P denotes the fixed power of the transmitter, $|h_{x_i}|^2$ is the fast fading power in the x_i-y link, $\ell(\cdot)$ represents the path loss function and $||x_i - y||$ is the distance between x_i and y. Due to Slivnyak's Theorem, $I(y)$ does not depend on the given

location where interference is measured, i.e., it does not matter whether y is part of the point process Φ or not. In (2.5), $I(y)$ is a shot-noise random variable because of the fast fading and the randomness in the point process.

Let $r_i = ||x_i - y||$, then $\Phi_r = \{r_i\}$ forms an inhomogeneous PPP with density function $\lambda(r) = 2\pi\lambda r$, since $||x_i - y||$ is the mapping of the homogeneous PPP to one dimension. Consider the unit transmit power and a path loss function $\ell(r) = r^{-\alpha}$, where α is the path loss exponent, we can then compute the Laplace transform of the interference [80, Sec. 5.1.7]

$$\mathcal{L}_I(s) = \mathbb{E}\left[e^{-sI}\right] = e^{-\pi\lambda\mathbb{E}(|h|^{4/\alpha})\Gamma(1-2/\alpha)s^{2/\alpha}}, \tag{2.6}$$

where $\Gamma(\cdot)$ is the Gamma function. The Laplace transform facilitates the computation of many network metrics such as coverage probability. Equation (2.6) has a closed-form expression in the case of Rayleigh fading by plugging in $\mathbb{E}(|h|^{4/\alpha}) = \Gamma(1+2/\alpha)$. It is worth noting that (2.6) exists only for $\alpha > 2$. If $\alpha \leq 2$, then $I(y) = \infty$, as the interference power from all far away transmitters does not decay fast enough and the PPP inherently considers a network in an infinite area. This is not a problem if a finite area is considered [82]–[84]. For $\alpha > 2$, $I(y)$ is finite but $\mathbb{E}(I(y)) = \infty$ [80, Sec. 5.1.2], since a transmitter that is very close to y causes high interference due to the singularity of the path loss law at y.

2.4 Coverage Analysis

The SINR for a user at the origin of a 2-dimensional plane with single antenna on both the BSs and the user sides is given by

$$\text{SINR} = \frac{P\ell(r_0)|h_0|^2}{\sum_{k\in\Phi,k\neq 0} P\ell(r_k)|h_k|^2 + \sigma^2}, \tag{2.7}$$

where r_0 denotes the distance to the associating BS, r_k represents the distance to the k-th interfering BS and σ^2 is the additive noise power. For a given modulation and coding scheme, a user is considered in coverage if the SINR exceeds a threshold T. For Rayleigh fading and unit transmit power, the coverage probability for a given link distance r_0 is given by [13, Eq. (2)]

$$\mathbb{P}\left(\text{SINR} > T|r_0\right) = e^{\left(-Tr_0^\alpha\sigma^2\right)}\mathbb{E}\left[e^{-Tr_0^\alpha I}\right]. \tag{2.8}$$

The expectation in (2.8) is the Laplace transform of the interference with $s = Tr_0^\alpha$. Combining (2.6) and (2.8), we have

$$\mathbb{P}\left(\text{SINR} > T|r_0\right) = e^{\left(-\lambda\pi r_0^2 T^\alpha \frac{2\pi/\alpha}{\sin(2\pi/\alpha)} - Tr_0^\alpha\sigma^2\right)}. \tag{2.9}$$

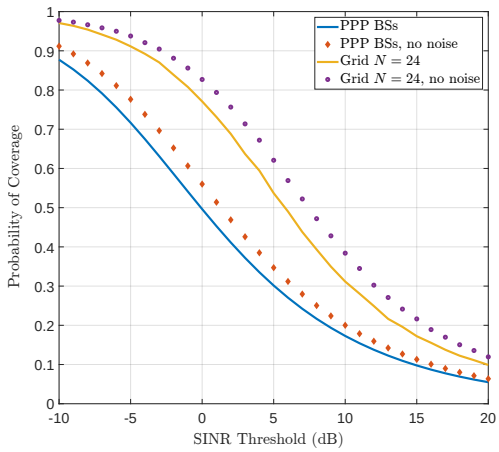

Figure 2.3: Coverage probability of the PPP model and the grid model as a function of coverage SINR threshold for $\alpha = 4$ and the interference-limited case.

In order to obtain the coverage probability for a typical user randomly placed in the PPP network, i.e., removing the conditioning on a given link distance r_0, we need to consider the BS association strategy and find the distribution of the link distance. Cell association strategies are usually based on link quality, traffic load requirements and location information. The simplest cell association strategy associates a user to the nearest BS. If the path loss model is given by $\ell(r) = r^{-\alpha}$, the nearest BS association gives the maximum signal power averaged over fading. The probability density function (PDF) of the link distance r based on the nearest BS association is given by [85]

$$f_r(r) = e^{-\lambda\pi r^2} 2\pi r. \tag{2.10}$$

Hence, the coverage probability of a typical user randomly placed in a network based on PPP is [13, Theorem 2]

$$\mathbb{P}\left(\text{SINR} > T\right) = \int_0^\infty \mathbb{P}\left(\text{SINR} > T | r_0\right) f_r(r_0)\, \mathrm{d}r_0, \tag{2.11}$$

$$= \pi\lambda \int_0^\infty e^{\left(-\lambda\pi v(1+\rho(T,\alpha)) - \mu T v^{\alpha/2}\sigma^2\right)} \mathrm{d}v, \tag{2.12}$$

where

$$\rho(T,\alpha) = T^{2/\alpha} \int_{T^{-2/\alpha}}^\infty \frac{1}{1+u^{\alpha/2}} \mathrm{d}u, \tag{2.13}$$

and $1/\mu$ is the fixed transmit power.

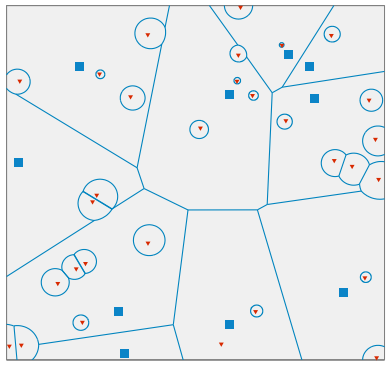

Figure 2.4: A realization of the coverage area in a heterogeneous network based on PPP. The blue squares and red triangles denote the macro and small BSs with descending transmit powers, respectively.

Figure 2.3 shows the coverage probability comparison between the PPP model [13, Theorem 2] and the grid model where N is the number of BSs in square grids with a fixed size. It confirms that, because the PPP model allows two BSs to get arbitrarily close, it gives pessimistic coverage probability, while the grid model gives optimistic results due to the fact that there is always a BS within a specified distance and never a strong interfering BS nearby. In reality, the BS deployment is expected to be less random than the PPP model and more irregular than the grid model. Hence, the coverage probability of a real BS deployment is likely to fall between that of the two models. Also, Fig. 2.3 shows the coverage probability of the interference-limited case where the noise is neglected, which confirms that, due to the large interference power in dense networks, the performance difference between the cases with noise and without noise is similar. In most cases, the interference-limited case can simplify the analysis and often leads to tractable analytical forms, therefore, neglecting noise is preferred in the performance analysis of dense networks.

For heterogeneous networks with K-tier BSs, the SINR of a typical user associated to a BS in tier k is given by

$$\mathrm{SINR}_k = \frac{P_k |h_{k,0}|^2 r^{-\alpha_k}}{\sum_{j=1}^{K} \sum_{i \in \Phi_j \setminus B_{k,0}} P_j |h_{j,i}|^2 r_{j,i}^{-\alpha_j} + \sigma^2}, \tag{2.14}$$

where P_j is the transmit power for tier-j BSs and $r_{j,i}$ is the distance between the user and BS i in the j-th tier. It is possible to derive the coverage probability of a typical user in K tier heterogeneous networks by following a similar procedure as that in the single-tier PPP network [24].

Figure 2.4 shows the coverage area of a heterogeneous network with large cells and small cells based on PPP and the nearest BS association, the coverage area forms a Voronoi tessellation where the boundaries have equal average received power from the nearest BSs and it resembles an actual network coverage area. It is worth noting that a bias factor can be added to the average received power model given by $B_i P_i r^{-\alpha_i}$, where B_i represents the bias towards associating to the i-th tier BSs. By associating users to the BS with the maximum biased received power averaged over fading, small BSs' coverage area can be expanded through increasing the bias factor, thus offloading to small BSs. Also, if the blocking effect is considered, the nearest BS does not necessarily provide the highest signal strength and serving a user by a BS with LOS connection may lead to better system performance.

Diversity combining techniques at the receiver side can reduce the effect of multi-path fading and shadowing. For heterogeneous networks, the interference power is often correlated due to the fact that different signal paths are caused by the same set of interfering sources. Therefore, it is interesting to study the performance of different types of diversity combining techniques where interference power and the spatial interference correlation are taken into account. Consider a multi-antenna system where the transmitters are modeled by a homogeneous PPP Φ, a receiver with N antennas is placed at the origin of a 2D plane and it receives signals from a transmitter x_0 at distance d. After combining, the SINR is given by

$$\text{SINR} = \frac{P_0 |\sum_{i=1}^{N} w_i h_i|^2 \ell(r_0)}{\sum_{i=1}^{N} \sum_{x_i \in \Phi_i} P_{x_i} \ell(r_{x_i}) |w_i h_{i,x}|^2 + \sigma^2}, \tag{2.15}$$

where Φ_i denotes the set of interfering transmitters picked up by the i-th antenna and P_0, P_{x_i} are the transmit power of the associated BS and the interfering BSs, respectively. In (2.15), it is assumed that each antenna receives interference from a fraction of the total interfering transmitters $\Phi_i \subseteq \Phi$. Despite of the independent fast fading, the interfering signals received on different antennas are correlated due to the fact that the spatial locations of some transmitters appear in different sets Φ_i [86], [87]. In a densely deployed network, the receiver SINR tends to be interference-limited and the additive noise is negligible compared to the total interference power. Hence, receiver signal-to-interference ratio (SIR) is an accurate performance metric for dense networks.

Considering the spatial correlation and Rayleigh fading, the SIR distribution can often be expressed in closed-form expressions for maximum-ratio combining (MRC), selection combining (SC), equal-gain combining (EGC) and switch-and-stay combining (SSC) using stochastic geometry. These combining techniques can improve the SIR by exploiting the channel diversity. MRC applies weights that are inversely proportional to the interferer density seen by each antenna, and the exact expression of the SIR distribution in the case of two antennas is given by [87, Theorem 1]. In [23],

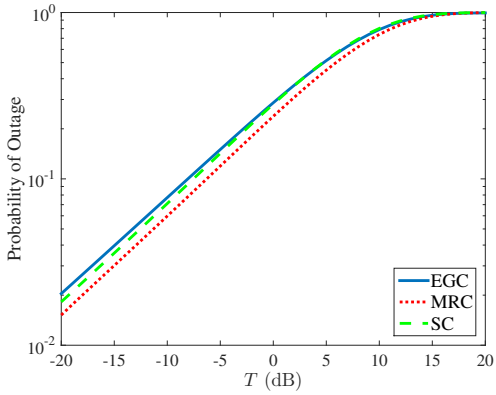

Figure 2.5: Probability of outage for EGC, MRC and SC as a function of outage threshold T. All interfering channels and the desired signal channel is assumed to have Rayleigh fading and path loss with path loss exponent $\alpha = 3.5$. The desired link distance is $d = 10$ m.

i.e., Paper C of Part 2 the exact SIR distribution for dual-antenna EGC where the received signal on each antenna are co-phased and equally weighted is given. For a large number of antennas, tight bounds can also be found in closed-form for MRC and EGC [23], [87]. These bounds are shown to have good accuracy in terms of coverage analysis. SC chooses the antenna with the best SIR and its distribution is given by [86, Eq. (8)]. SSC is the simplest combining technique where the combiner switches to, and stays with, one receive antenna as long as the SIR on that antenna is above a predetermined threshold, regardless of the interference condition on the other antennas, the SIR distribution of SSC-based receivers can be found in Sec. 5.3.1.

Figure 2.5 compares the outage probability (complementary cumulative distribution function (CCDF) of the SIR) for MRC, EGC and SC in the cases with two receiver antennas. As shown in Sec. 5.3.1, SC is considered as the optimal case of SSC, in terms of the outage probability, the performance of the SSC is omitted in the comparison. From Fig. 2.5, we observe that MRC has the best performance and EGC performs slightly worse than SC. An intuitive explanation is that, different from the interference-free case, the diversity exits not only in the useful signal power but also in the interference power. By combining the signals of all antennas. The EGC may suffer from adding up the antennas with large interference power. While for SC, antennas with poor SIR are automatically ignored, and for the MRC scheme, weights are used to compensate for the interference-affected antennas.

The coverage probability can be further improved by hybrid automatic repeat request (HARQ). As an example method, let us consider the incremental redundancy (INR) ARQ, as a practical scheme already implemented in many standards[60], [88]–

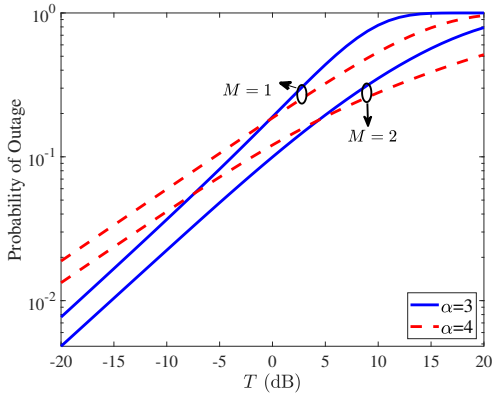

Figure 2.6: Probability of outage for EGC with different values of the path loss exponent as a function of outage threshold T. Also, the probability of outage in connection with hybrid ARQ is given for maximum number of transmissions $M = 1$ and $M = 2$. All interfering channels and the desired signal channel are assumed to have Rayleigh fading, and path loss with path loss exponent $\alpha = 3.5$. The desired link distance is $d = 10$, and the number of antennas is $N = 4$.

[90]. Considering INR ARQ with a maximum of M transmission rounds, the codeword is partitioned into M subcodewords. Then, the subcodewords are transmitted in successive rounds until the receiver correctly decodes the data or the maximum permitted transmission round is reached. Also, in each round the receiver combines all signals received up to the end of that round to decode the message. In this way, considering block fading conditions where the channel coefficients remain constant during the retransmissions, the coverage probability is given by [88]–[90]

$$\Pr(\text{Outage})_{\text{A,INR},M} = 1 - \Pr\left(\log(1+\text{SIR}_\text{A}) < \frac{\log(1+T)}{M}\right), \quad \text{A} = \{\text{SSC}, \text{SC}, \text{MRC}, \text{EGC}\}, \tag{2.16}$$

where $\log(1+T)$ denotes the rate of the initial subcodeword.

Figure 2.6 shows the improvements by employing the HARQ with $M = 2$. Thus, the figure emphasizes the importance of using performance-enhancing techniques for dense networks. The more detailed performance analysis of HARQ-based dense networks is an interesting extension topic. In addition, Figure 2.6 illustrates the effect of the path loss exponent on the outage probability. We observe that a higher path loss causes additional/less outage when T is small/large. This is because the interference power reduces faster than the desired signal power. Also, the observation indicates that, in order to maintain a sufficiently low target outage probability in an area with high path loss, it is better to set T, hence the transmission rate $\log(1+T)$,

small.

In [91], we study the partial-zero-forcing receiver which cancels some of the strongest interference signals and uses the remaining degrees of freedom of the antennas for useful signal enhancement. The received SINR for the partial-zero-forcing receiver is given by

$$\mathrm{SINR} = \frac{P_0 |\mathbf{v}_0^H \mathbf{h}_0|^2 \ell(r_0)}{\sum_{k=K+1}^{\infty} P_k \ell(r_k) |\mathbf{v}_0^H \mathbf{h}_k|^2 + \sigma^2}, \tag{2.17}$$

where $\mathbf{v}_0, \mathbf{v}_k$ denote the combining weights at the receiver for the associating BS and the interfering BSs, respectively. Here, the interfering transmitters are sorted in a descending order in terms of the average received power. The partial-zero-forcing eliminates the K strongest interferers while maximizing the useful signal power. The SINR distribution for the partial-zero-forcing receiver is given by[91, Eq.(16)].

The same framework can be applied to find tractable expressions for the coverage probability considering emerging 5G technologies such as massive MIMO [92], non-orthogonal multiple access (NOMA) [93] and self-backhauled networks [94].

2.5 Throughput and Area Spectral Efficiency

When no channel state information (CSI) is assumed at the BSs, each BS selects a transmission rate $R = \log(1 + T)$ with T being an auxiliary variable. If the instantaneous SINR supports the rate, the signal can be successfully decoded at the user and the user is in coverage. Applying the result of the coverage probability, the per-user throughput is given by

$$\eta = \log(1 + T)\mathbb{P}\left(\mathrm{SINR} > T\right). \tag{2.18}$$

The per-user throughput does not monotonically increase with T, as the coverage probability decreases if the transmission rate is too large, and there exists an optimal T that maximizes the throughput. In [95], we derive the closed-form optimal transmission rate maximizing the throughput in PPP networks. The same approach can be used to analyze the area spectral efficiency, which is the throughput normalized by the cell area. In [Paper C, Eq. (16)], we give the optimal BS density maximizing the area spectral efficiency, and we study the delay-limited area spectral efficiency in [96]. Here, delay-limited area spectral efficiency is defined as the ratio between the achievable throughput and the affected area, i.e., the area where a significant amount of transmission power is observed. For EGC, the per-user throughput is further studied in Sec. 5.3.

CHAPTER 3

Multi-cell mmWave Systems

As the density of the BSs keeps growing, inter-cell and intra-cell interference management is a key feature for achieving high-capacity multi-stream transmissions. Many network interference management methods aim to eliminate interference caused by adjacent transmitting BSs. In particular, CoMP techniques exploit both the time and spatial diversity so that signals transmitted from multiple BSs do not cause serious interference to each others' serving users. CoMP techniques were first specified in LTE-Advanced (LTE-A) for both the intra- and inter-BS systems with ideal and non-ideal backhaul[97]. In 5G systems, network services, spectrum and deployments have become more diverse than before. In order to satisfy the service requirements of enhanced mobile broadband, mission-critical communications and massive Internet-of-Things (IoT), CoMP techniques should provide a unified solution by coordinating multiple BSs of different types and spectrum to achieve high capacity, low latency and high reliability. In mmWave systems, since BSs tend to be equipped with large antenna arrays, CoMP techniques should consider high-gain beamforming and jointly optimize beamformers for high network capacity.

To realize CoMP techniques often requires dedicated CSI feedback and control signaling. The high hardware complexity and large data size of CSI, which are associated with large antenna arrays, add more challenges to CoMP design. For the conventional fully digital beamforming architecture, hardware such as digital-to-analog converters (DACs)/analog-to-digital converters (ADCs) and RF chains increases with the number of antennas. To reduce the number of RF chains and DACs/ADCs, the hybrid beamforming architecture, where each antenna is connected through phase shifters (PSs) to fewer number of RF chains, is preferred. CoMP techniques for fully digital

beamforming have been studied extensively in the literature [98]–[101]. Due to the additional constraints of hybrid beamforming architectures, CoMP techniques need to jointly design both the analog and the digital precoders and combiners. Early work on the topic of joint hybrid beamforming design in mmWave systems is based on the channel eigenvalues [53] and the measurement data of diversity and CoMP techniques [102]. Thus, for CoMP to be realized and achieve high spectral and energy efficiency, some of the key challenges lie in finding efficient beamforming methods that exploit multi-user CSI and joint optimizations for transmitting from multiple BSs.

In this chapter, we introduce the CoMP transmission schemes in mmWave systems. In particular, we present the categories of CoMP schemes in Sec. 3.1 and the general optimization tools used in CoMP schemes in Sec. 3.2. Finally, the modeling of joint hybrid beamforming in multi-user and multi-BS setups is given in Sec. 3.3.

3.1 Downlink CoMP Strategies

For downlink multi-cell cooperation, it is often required that the BSs are mutually connected or centrally controlled by a coordination unit, so that CSI and control signals can be gathered from all BSs to make joint decisions on transmission parameters such as user scheduling, beamforming, transmit power, etc. CoMP techniques can be categorized based on the availability of data symbols of a user at each coordinated BS [97], [103], [104]:

- *Coordinated scheduling/beamforming*: Each user is served by only one BS and the data intended for a user is only available at the serving BS. Decisions on user scheduling or beamforming are made according to the CSI of both direct and interfering links and the system quality-of-service (QoS) requirements. By jointly computing the beamforming precoders at each BS, the interference signal can be steered toward the null space of the receiver, thus reducing interference power experienced by users. Other coordinated beamforming methods that require lower feedback overhead or CSI accuracy than joint beamforming rely on predefined codebooks. In this case the BSs can select beamforming precoders from a codebook based on certain performance requirements and channel conditions.
- *Joint processing*: If each user can be served by more than one BS, joint processing enables simultaneous data transmissions from multiple BSs to a single user. The signals received from multiple BSs can be combined to improve the received signal quality rather than being treated as interference. In this case, the transmit data for the user should be available at multiple BSs and the CSI from multiple BSs should be considered together to jointly design beamforming precoders and combiners. However, backhaul constraints, scheduling complexity and beamforming computational complexity may limit the BS coordination size. A special case of joint processing, *dynamic point selection*, restricts the data to

be transmitted from one BS in a time-frequency resource, but the transmitting BS is dynamically selected among the coordinated BSs in each subframe, while the data symbols are available at multiple coordinated BSs. The dynamic point selection schedules the most appropriate BS by a predefined metric according to changes in the channel fading and blockage conditions.

- *Relay-assisted cooperation*: In contrast to cooperation among BSs, the relay-assisted cooperation adds dedicated relay nodes inside a cell and with no need for connections to other BSs. The transmit data is firstly received and processed at a relay node before being forwarded to the user. Such relay nodes also allow for simplest cooperation is the amplify-and-forward type which, however, amplifies both the useful signal power and the interference plus noise power. More advanced relay nodes decode and further process the data, such as data concatenation/segmentation, before encoding and forwarding to the user, thus allowing more control functions at the relay node to e.g. avoid amplifying noise and interference..

CoMP techniques aim at serving a user with multiple BSs without excessive inter-cell interference. The downlink data can be scheduled at multiple BSs and be transmitted in the same time-frequency recourse blocks by exploiting the interference channel. However, the performance gain of CoMP schemes largely depends on the level of synchronization among the BSs, CSI feedback and backhaul quality. Generally, the CSI feedback of a user from multiple BSs is needed for coordinated shceduling/beamforming and joint processing. Additional information such as phase synchronization for joint processing with coherent combining is needed for higher level cooperation. Backhaul capacity and quality are also important for having the transmit data available at multiple BSs and the exchange of CSI among BSs. Especially for dense mmWave networks, where a mixture of high-capacity wireless backhaul links and fixed fiber backhaul links between BSs are expected, both access and backhaul links will be subject to wireless channel quality. Hence, the impact of CSI and control message overhead, the quality of the feedback channels and the introduced latency need to be considered for realizing the full capacity of CoMP.

3.2 Resource Allocation in CoMP

Efficient allocation of resources is the key to maximize the network-level energy and spectral efficiency and guarantee service reliability. In general, multi-cell multi-user networks can be modeled as a large multi-user MIMO system, where users are jointly served by all BSs. Such a model was originally proposed and investigated in [105], and denoted Network MIMO in [106]. In CoMP networks, radio resources including time, frequency, power, and rate need to be allocated among a set of clustered collaborative BSs and associated users. The resource allocation problem is usually formulated as optimizations over network data rate or power consumption with con-

straints on transmit power per antenna and per-user data rate. In recent works, the Network MIMO and CoMP concepts have been generalized to cell-free MIMO [107], [108], in which the cellular structure is relaxed and the BSs can be split into access points (APs), with various levels of reduced functionality compared to a BS, and a central processing units (CPU). Further generalization of the concept is currently under investigation and denoted distributed MIMO (D-MIMO) Systems, in which multiple CPUs can coordinate overlapping clusters of APs with converged backhaul-fronthauling [109].

In this subsection, we present several common resource allocation problems and discuss their applications in dense mmWave networks. It is worth noting that, as discussed in Sec. 3.1, we make assumptions on ideal synchronization, CSI acquisition, backhaul and possible fronthaul to central processing units when discussing system models. Here, the purpose is to understand the theoretical resource allocation algorithms in CoMP.

3.2.1 System Model

Considering a network with M BSs, each equipped with N antennas, and K single-antenna users, the channel between user k and BS m is denoted by $\mathbf{h}_{k,m} \in \mathbb{C}^N$ and is assumed to be block fading channel. The received complex signal at user k is given by

$$y_k = \sum_{m=1}^{M} \mathbf{h}_{k,m}^{\mathrm{H}} \mathbf{w}_{k,m} x_{k,m} + \sum_{m=1}^{M} \sum_{k' \neq k, k'=1}^{K} \mathbf{h}_{k,m}^{\mathrm{H}} \mathbf{w}_{k',m} x_{k',m} + n_k, \tag{3.1}$$

where $x_{k,m}$ is the normalized, intended and random transmitted signal with $\mathbb{E}[|x_{k,m}|^2] = 1$, $\mathbf{w}_{k,M} \in \mathbb{C}^N$ is the precoding vector, and $n_k \sim \mathcal{CN}(0, \sigma_k^2)$ is the additive noise. The first term in (3.1) represents the desired signal transmitted from all serving BSs and the second term is the interference signal from the BSs transmitting to other users.

Depending on users' locations and channel quality, it may not be optimal for user k to be served by all BSs. Denoting the set of serving BSs for user k as $\mathcal{M}_k$, the effective transmit signal power from a given BS is 0 if $\mathbf{w}_{k,m} = \mathbf{0}$, if $m \notin \mathcal{M}_k$. Therefore, resource allocation optimization give the precoding vectors as well as the serving BS sets by checking non-zero precoders.

To provide a general introduction to different resource allocation algorithms, next, we simplify the model to the single-cell multi-user case and denote the desired transmit power for user k as $p_{k,m} = ||\mathbf{w}_{k,m}||^2$ and, the effective SINR of user k is then given by [108, Eq. (3.31)]

$$\mathrm{SINR}_k = \frac{|s(p_{k,m})|^2}{\sum_{k' \neq k, k'=1}^{K} \mathbb{E}[|I_{k',m}(p_{k',m})|^2] + \sigma_k^2}, \tag{3.2}$$

Algorithm 1 Bisection algorithm

Require: Objective improvement accuracy $\epsilon > 0$

1: Set the lower bound and upper bound on the max-min SINR as $t^{\text{lower}} \leftarrow 0$ and $t^{\text{upper}} \leftarrow \min_k \max_{\mathbf{p} \geq \mathbf{0}} \text{SINR}_k(\text{p})$
2: Set initial solution $\mathbf{p}^{\text{opt}} = \mathbf{0}, t^{\text{opt}} = 0$
3: **repeat**
4: $t^{\text{candidate}} \leftarrow \frac{t^{\text{upper}} + t^{\text{lower}}}{2}$
5: Solve the following problem:

$$\begin{aligned} & \min_{\mathbf{p} \geq \mathbf{0}} \sum_{k=1}^{K} p_k \\ s.t. \quad & \text{SINR}_k(\mathbf{p}) \geq t^{\text{candidate}}, \forall k, \\ & \mathbf{a}_r^{\text{T}} \mathbf{p} \leq p_{\max}, r = 1, \cdots, R \\ & \mathbf{p} \geq \mathbf{0} \end{aligned} \tag{3.3}$$

6: **if** (3.3) is feasible **then**
7: $t^{\text{lower}} \leftarrow t^{\text{candidate}}, \mathbf{p}^{\text{opt}} = \mathbf{p}$
8: **else**
9: $t^{\text{upper}} \leftarrow t^{\text{candidate}}$
10: **until** $t^{\text{upper}} - t^{\text{lower}} < \epsilon$

where $s(p_{k,m})$ is the complex useful signal amplitude and $I_{k',m}(p_{k',m}) = \mathbf{h}_{k,m}^{\text{H}} \mathbf{w}_{k',m}$ is the complex interference signal amplitude. Clearly, (3.2) is a function of $\mathbf{p} = [p_{1,m}, \ldots, p_{K,m}]$, denoting (3.2) as $\text{SINR}_k(\mathbf{p})$, the achievable spectral efficiency can be written as $\text{SE}_k(\mathbf{p}) = \log_2(1 + \text{SINR}_k(\mathbf{p}))$. To optimize the network performance, a vector containing the spectral efficiency of all users $[\text{SE}_1(\mathbf{p}), \ldots, \text{SE}_K(\mathbf{p})]$ needs to be considered by allocating transmit power, hence optimizing precoding vectors, to different users. Depending on the objectives and constraints of a specific network, different algorithms and results can be obtained. In the rest of the subsection, we introduce the classic resource allocation problems of max-min spectral efficiency fairness and sum spectral efficiency maximization.

3.2.2 Max-Min Spectral Efficiency Fairness

In max-min spectral efficiency fairness problems, the worst user spectral efficiency is maximized to achieve fairness among users. The problem can be expressed as [108, Eq.(3.33)]

$$\mathcal{P}_1 : \quad \max_{\mathbf{p} \geq \mathbf{0}} \min_k \text{SINR}_k(\mathbf{p}), \tag{3.4}$$

$$\text{s.t.} \quad \mathbf{a}_r^{\text{T}} \mathbf{p} \leq p_{\max}, r = 1, \ldots, R, \tag{3.5}$$

where the R constraints limit the sum of the weighted power to be below the maximum allowed power $p_{\max}$ and $\mathbf{a}_r \in \mathbb{R}^K$ is the weighting vector. Problem $\mathcal{P}_1$ can be transformed to the following linear problem by introducing an auxiliary parameter t, we have

$$\mathcal{P}_2 : \max_{\mathbf{p}\geq\mathbf{0}, t\geq 0} t \tag{3.6}$$

$$\text{s.t. } \mathrm{SINR}_k(\mathbf{p}) \geq t, \forall k, \tag{3.7}$$

$$\mathbf{a}_r^{\mathrm{T}}\mathbf{p} \leq p_{\max}, r = 1, \ldots, R. \tag{3.8}$$

Here, t represents the lowest SINR among all users. Problem P_2 should give the same optimal power allocation as Problem P_1 [110] and the optimal solution can be obtained by using the bisection method described in [108, Algorithm 3.1]. The algorithm iteratively updates t and $\mathbf{p}$ until a local optimal is found.

3.2.3 Sum Spectral Efficiency Maximization

The max-min spectral efficiency problem aims to achieve similar spectral efficiency among users and focuses on the worst users performance. In scenarios where the majority of the users can have large spectral efficiency without introducing extra interference to the users experiencing bad channel conditions, it is beneficial to maximize the sum of the spectral efficiency. The sum spectral efficiency maximization problem can be expressed as

$$\mathcal{P}_3 : \max_{\mathbf{p}\geq\mathbf{0}} \sum_{k=1}^{K} \log_2(1 + \mathrm{SINR}_k(\mathbf{p})), \tag{3.9}$$

$$\text{s.t. } \mathbf{a}_r^{\mathrm{T}}\mathbf{p} \leq p_{\max}, r = 1, \ldots, R. \tag{3.10}$$

Problem $\mathcal{P}_3$ is usually non-convex and requires impractically high-complexity methods to find the global optima. Realistic methods often involve iterative algorithms that give a local optima and the optimization problems can be solved in a limited amount of time. Problem $\mathcal{P}_3$ can be reformulated to a weighted MMSE (minimum mean square error) problem and it is shown that the weighted MMSE problem has the same global optimal solution as the original problem [108].

Defining the estimate of the desired signal x_k at the receiver as $\hat{x}_k = u_k^* y_k, u_k \in \mathbb{C}$, the MSE (mean square error) is given by

$$\begin{aligned} e_k(\mathbf{p}, u_k) &= \mathbb{E}[|\hat{x}_k - x_k|^2] \\ &= |u_k|^2(|s(p_{k,m})|^2 + \sum_{k'\neq k, k'=1}^{K} \mathbb{E}[|I_{k',m}(p_{k',m})|^2] + \sigma^2) - 2\Re(u_k^* s(k,m)) + 1. \end{aligned} \tag{3.11}$$

Introducing an auxiliary parameter $d_k > 0$, the following problem is equivalent to Problem $\mathcal{P}_3$:

$$\mathcal{P}_4 \min_{\mathbf{p}\geq\mathbf{0},\{d_k,u_k\geq 0,\forall k\}} \sum_{k=1}^{K}(d_k e_k(\mathbf{p},u_k) - \ln(d_k)) \tag{3.12}$$

$$\text{s.t.} \mathbf{a}_r^{\mathrm{T}}\mathbf{p} \leq p_{\max}, r = 1,\ldots,R. \tag{3.13}$$

The benefit of transforming Problem $\mathcal{P}_3$ to $\mathcal{P}_4$ is that it can be efficiently solved by the block coordinate descent algorithm which is sketched in [108, Algorithm 3.3]. The variables u_k, d_k and $\mathbf{p}$ are alternately updated until a local optima $\mathbf{p}$ is found.

3.3 Resource Allocation in Cooperative mmWave Systems

5G systems with mmWave small cells will enable CoMP with multi-layer connectivity resulting in high data rates. One of the main differences between CoMP in mmWave and sub-6G GHz communications is due to the beamforming architecture. Equipped with large antenna arrays, mmWave systems with hybrid beamforming architecture have the advantage of reduced hardware cost with little or no performance loss. The hybrid beamforming architecture requires to jointly design the analog and digital beamforming. Optimal hybrid beamforming design for capacity maximization involves non-convex problems [41], [44]. Thus, algorithm development for CoMP in mmWave systems should reduce the complexity of joint beamforming design and improve the performance of currently proposed hybrid beamforming schemes. In addition, CoMP schemes need to exploit mmWave channel characteristics to reduce the interference power and ensure close to LOS transmissions.

In the following, we present the system model of a multi-tier cooperative mmWave network where joint processing is possible. Because one of the key features of 5G is system sustainability, joint hybrid precoding schemes are proposed in Paper A to minimize the total power consumption of the network while satisfying a per-user rate constraint.

3.3.1 Hybrid Precoding Architecture

Consider a downlink multi-tier mmWave network consisting of M multi-antenna BSs and K single-antenna users. BSs in different tiers are differentiated by the number of antennas, RF chains and maximum RF transmit power. Denote the number of RF chains and the number of antennas at BS m by L_m and N_m, respectively. Furthermore, denote the precoder at BS m for user k by $\mathbf{w}_{k,m} = \mathbf{R}_m\mathbf{d}_{k,m}$, where $\mathbf{d}_{k,m} \in \mathbb{C}^{L_m}$ is the digital precoder and $\mathbf{R}_m \in \left\{\mathbf{R}_m \in \mathbb{C}^{N_m\times L_m} \middle| \left|\mathbf{R}_m^{(i,j)}\right| = \frac{1}{\sqrt{N_m L_m}}\right\}$

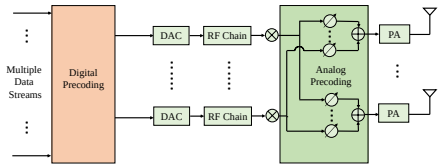

Figure 3.1: Fully-connected hybrid precoding architecture.

is the analog precoder. The analog precoder has an equal magnitude constraint as it is implemented by PSs. In the case of joint processing, a user can receive multiple streams from different BSs concurrently, and the composite received signal at UE k is given by

$$y_k = \sum_{m=1}^{M} \mathbf{h}_{k,m}\mathbf{R}_m\mathbf{d}_{k,m}x_{k,m} + \sum_{m=1}^{M}\sum_{k'\neq k,k'=1}^{K} \mathbf{h}_{k,m}\mathbf{R}_m\mathbf{d}_{k',m}x_{k',m} + n_k, \tag{3.14}$$

If BS m is not associated with UE k in the joint transmission, it can be simply treated as $\mathbf{R}_m\mathbf{d}_{k,m} = \mathbf{0}$.

Assume that the data symbols are mutually independent and the user applies successive interference cancellation (SIC) to sequentially decode the strongest signal and subtract it from the composite signal. Furthermore, assume Gaussian signaling, the achievable spectral efficiency of UE y is given by

$$\eta_k = \log_2\left(1 + \frac{\sum_{m=1}^{M} |\mathbf{h}_{k,m}^H\mathbf{R}_m\mathbf{d}_{k,m}|^2}{I_k + \sigma_k^2}\right), \tag{3.15}$$

where

$$I_k = \sum_{m=1}^{M}\sum_{k'\neq k,k'=1}^{K} \mathbf{d}_{k',m}^H\mathbf{R}_m^H\mathbf{h}_{k,m}\mathbf{h}_{k,m}^H\mathbf{R}_m\mathbf{d}_{k',m} \tag{3.16}$$

is the interference power.

One of the main differences between the hybrid and the fully-digital precoding (FDP) architectures is the hardware and its associated power consumption. To compare the power consumption, considering only DACs, RF chains and PSs [45], as shown in Fig. 3.1, the hybrid precoding architecture requires L_m additional PSs per antenna but $(N_m - L_m)$ less digital-to-analog converters (DACs) and RF chains compared to the FDP architecture.

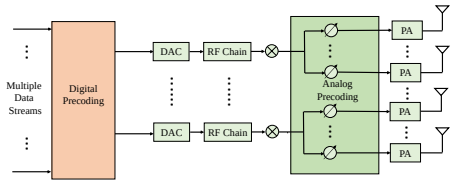

Figure 3.2: Partially-connected hybrid precoding architecture.

Depending on the extent of interconnections and the number of PSs needed, the hybrid precoding architectures can be further categorized into the fully-connected hybrid precoding (FHP) and the partially-connected hybrid precoding (PHP) architectures. As shown in Fig. 3.2, the PHP architecture reduces the number of PSs and the interconnections between the RF chains and the antennas by connecting each RF chain to an antenna subarray, within which each antenna is connected to one PS. For the PHP, we additionally assume that $N_m/L_m, \forall m$, is an integer such that each RF chain is connected to an antenna subarray and they do not overlap. Hence, the number of PSs required in the FHP is $L_m N_m$ and it is reduced to N_m in the PHP. For the FDP architecture, because $N_m = L_m$, PSs are not needed to connect the antennas and RF chains.

For FHP, the entries in the analog precoder have the constant amplitude constraint $\left|\mathbf{R}_m^{(i,j)}\right| = \frac{1}{\sqrt{L_m N_m}}, \forall m$. For PHP, each RF chain is connected to part of the PSs, therefore the analog precoder has the form of a block diagonal matrix given by $\mathbf{R}_m = \text{diag}[\hat{\mathbf{r}}_{1,m}, \cdots, \hat{\mathbf{r}}_{L_m,m}]$, where $\hat{\mathbf{r}}_{i,m} \in \mathbb{C}^{N_m/L_m \times 1}, 1 \leq i \leq L_m$, with constraints $\left|\hat{\mathbf{r}}_{i,m}^{(j)}\right| = 1/\sqrt{N_m}, \forall m$. Considering the power consumption from hardware, the total power consumption of the hybrid beamforming architecture at a BS can be modeled by

$$P_m^{\text{HB}} = \Delta_m \sum_{k=1}^{K} ||\mathbf{R}_m \mathbf{d}_{k,m}||^2 + L_m N_m P_{\text{ps}} + L_m \left(P_{\text{DAC}} + P_{\text{RF}}\right) + P_{\text{fix},m}, \tag{3.17}$$

and the total power consumption of the FDP architecture is given by

$$P_m^{\text{FD}} = \Delta_m \sum_{k=1}^{K} ||\mathbf{R}_m \mathbf{d}_{k,m}||^2 + N_m \left(P_{\text{DAC}} + P_{\text{RF}}\right) + P_{\text{fix},m}. \tag{3.18}$$

In (3.17) and (3.18), $\Delta_m \sum_{k=1}^{K} ||\mathbf{R}_m \mathbf{d}_{k,m}||^2$ is the power consumption at the amplifier and Δ_m models the power amplifier inefficiency. Then, $P_{\text{ps}}, P_{\text{DAC}}$ and P_{RF} denote the power consumption of the PSs, DACs and RF chains, respectively. Furthermore,

$P_{\text{fix},m}$ denotes the power dissipated at various other places, such as the power supply, cooling and backhaul maintenance.

Another mechanism which can greatly increase the power saving is to coordinate BSs' sleep and active mode such that the BS should be operational only when there is data to transmit. Depending on the latency requirement on the deactivation and reactivation, some hardware components may need to remain active during the sleep mode. Considering the BS active/sleep mode, the power consumption is modeled by

$$P_m = \begin{cases} P_m^{\text{HB/FD}}, & \text{active mode} \\ aP_m^{\text{HB/FD}}, & a \in [0,1] \ , \ \text{sleep mode.} \end{cases} \tag{3.19}$$

Note that in sleep mode, BSs do not serve the users, hence $\Delta_m \sum_{k=1}^{K} ||\mathbf{R}_m \mathbf{d}_{k,m}||^2 = 0$.

To fulfill the target of designing energy-efficient mmWave systems, one objective is to minimize the total power consumption of all BSs while guaranteeing the QoS for each user. By jointly designing the hybrid precoders, the optimal power allocation and BS sleep strategy can be obtained. The problem can be described as the follows:

$$\mathcal{P}_5 : \min_{\mathbf{R}_m \mathbf{d}_{k,m}} \sum_{m=1}^{M} b_m P_m \tag{3.20}$$

$$\text{s.t.} \quad \eta_k \geq \tau_k, \qquad \forall k \tag{3.21}$$

$$\sum_{k=1}^{K} ||\mathbf{R}_m \mathbf{d}_{k,m}||^2 \leq P_{\max,m}, \qquad \forall m \tag{3.22}$$

$$\left|\mathbf{R}_m^{(i,j)}\right| = \frac{1}{\sqrt{N_m L_m}}, \qquad \forall m,i,j, \qquad \text{for FHP,} \tag{3.23}$$

$$\mathbf{R}_m = \text{diag}[\hat{\mathbf{r}}_{1,m}, \cdots, \hat{\mathbf{r}}_{L_m,m}], \ \left|\hat{\mathbf{r}}_{i,m}^{(j)}\right| = 1/\sqrt{N_m}, \qquad \forall m,j, \qquad \text{for PHP,} \tag{3.24}$$

where b_m is the weighting parameter for balancing the load of BSs, τ_k is the minimum acceptable spectral efficiency for user k and can be used to ensure fairness among users, and $P_{\max,m}$ is the peak power limit of BS m. The solution to problem $\mathcal{P}_5$ gives the analog precoder for each BS and the digital precoder for each BS-user pair. It also reflects the UE association strategy, as the set of associated UEs of BS m is given by $\mathcal{K}_m = \{k | 0 \leq k \leq K, ||\mathbf{R}_m \mathbf{d}_{k,m}||^2 > 0\}$ and the set of serving BSs of UE k is given by $\mathcal{M}_k = \{m | 0 < m \leq M, ||\mathbf{R}_m \mathbf{d}_{k,m}||^2 > 0\}$.

The optimal solution to Problem $\mathcal{P}_5$ is not tractable due to the non-convex analog precoder constraint (3.23). Hence, suboptimal hybrid precoding methods [41]–[45], [111] are often based on disjoint analog and digital precoders design. In Paper A, i.e. [55], we decouple Problem $\mathcal{P}_5$ into an equal gain transmission problem, where analog precoders are found based on maximizing the useful signal power and a relaxed convex semi-definite problem which gives the digital precoders that solve Problem $\mathcal{P}_5$ conditioned on the analog precoders. The power consumption is compared to that

of the FDP architecture for which precoders are obtained by setting $L_m = N_m$ and removing the analog constraint (3.23) in Problem $\mathcal{P}_5$.

3.4 mmWave Channel Model

Measurements of mmWave channels have shown that many parameter statistics are different from sub-6 GHz signals. For example, the penetration loss of mmWave signals can be as high as 40 dB for a tinted glass in 28 GHz, and the diffuse scattering from rough surfaces causes large channel variations over short distance [112]. Also, the mmWave signal power can change dramatically from LOS to NLOS and human blockage can cause more than 40 dB fading [112]. Understanding the mmWave channel characteristics will help researchers to develop proper channel models, link adaptation and beamforming algorithms for performance enhancement. In this subsection, we present mmWave channel models that are commonly used for simulations.

Due to the fact that the angular spread is smaller in mmWave channels, compared to lower frequency channels, there may be a few dominant multi-path clusters with many subpaths of similar power, delay and angles. Thus, mmWave channel can be modeled by the Saleh-Valenzuela model, where we denote the channel vector between BS m and user k by

$$\mathbf{h}_{k,m} = \sqrt{\frac{l_{k,m} N_m}{N_{\text{cl}} N_{\text{ray}}}} \sum_{i=1}^{N_{\text{cl}}} \sum_{l=1}^{N_{\text{ray}}} \beta_{i,l} \mathbf{a}_m(\alpha_{i,l}). \tag{3.25}$$

Here, $l_{k,m}$ denotes the path loss, N_{cl} is the number of scattering clusters and N_{ray} represents the number of multipaths within a cluster. Also, $\beta_{i,l} \sim \mathcal{CN}(0,1)$ is the amplitude of the l-th path in the i-th cluster and $\mathbf{a}_m(\alpha_{i,l})$ denotes the antenna array response vector evaluated at the angle of departure $\alpha_{i,l}$. Depending on the antenna geometry, various array response vectors have been proposed. For simplicity, we adopt the linear array antennas whose response vector is given by

$$\mathbf{a}_m(\alpha_{i,l}) = \frac{1}{\sqrt{N_m}} \left[1, e^{jkd\sin(\alpha_{i,l})}, ..., e^{jkd(N_m-1)\sin(\alpha_{i,l})}\right]^T, \tag{3.26}$$

where $k = 2\pi/\lambda$, λ is the wavelength, $d = \lambda/2$ is the antenna spacing and $\alpha_{i,l}$ is assumed to follow a truncated Laplace distribution with mean cluster angle $\bar{\alpha}_i$ and angular spread σ_{α_i}. The mean cluster angle can be modeled by a uniform distribution $\mathcal{U}(\alpha_v^{\min}, \alpha_v^{\max})$, where $\alpha_v^{\min}$ and $\alpha_v^{\max}$ can be used to define the sector angular range.

There are numerous large-scale path loss models proposed for mmWave communications. In general, the parameters of the path loss models vary according to the scenarios and the frequency. For mmWave communications, the path loss model should differentiate between LOS and NLOS paths, as the signal power can be significantly different. Here, we present a collection of well adopted path loss models.

- *Path loss model with blocking* [16]: In order to show the difference between LOS and NLOS signal power, the path loss can be modeled as

$$l_{k,m} = \mathbb{I}(p_{\text{LOS}}(d_{k,m}))C_L d_{k,m}^{-\alpha_L} + (1 - \mathbb{I}(p_{\text{NLOS}}(d_{k,m})))C_N d_{k,m}^{-\alpha_N}. \tag{3.27}$$

  Here, $\mathbb{I}(p_L(r))$ is a Bernoulli random variable with LOS probability $p_L(r)$, α_L, α_N and C_L, C_N denote the path loss exponents and path loss at a reference distance for LOS and NLOS links, respectively. In [16], the LOS probability function is given by $p_{\text{LOS}}(d_{k,m}) = e^{-\beta d_{k,m}}$ where β is used to fit the model with different environments. The 3GPP LOS probability models are given by piece-wise functions [113]. The LOS probability is 1 if the distance is smaller than a threshold, otherwise it decays exponentially with distance.
- *Multi-slope path loss model*[114]: Standard Friis path loss model with one path loss exponent leads to unrealistic results in many scenarios, the multi-slope path loss model changes the path loss exponent according to the distance by

$$l_{k,m} = K_n d_{k,m}^{-\alpha_n}. \tag{3.28}$$

  Here, $d_{k,m}$ is the distance between user k and BS m, $K_n = \prod_{i=1}^{n} R_i^{\alpha_i - \alpha_{i-1}}$ and R_i is a critical distance beyond which the path loss exponent changes.
- *3GPP-based path loss model* [113]: This path loss model is defined separately for LOS and NLOS paths and is based on field measurements. For example, the LOS model of urban micro-cells is given by

$$l_{k,m}^{\text{LOS}} = \begin{cases} \text{PL}_1, & 10\text{m} \le d_{k,m} \le d \\ \text{PL}_2, & d \le d_{k,m} \le d_{\max}, \end{cases} \tag{3.29}$$

  where

$$\text{PL}_i = A_i + B_i \log_{10}(d_{k,m}) + 20 \log_{10}(f_c) + C_i, \qquad i = \{1, 2\}. \tag{3.30}$$

  Here, $d, d_{\max}, A_i, B_i, C_i$ are cell specific parameters and f_c is the carrier frequency.
- *Probabilistic path loss model* [115]: In order to generalize the path loss model to average the LOS and NLOS conditions, a weighting parameter, which is a function of the LOS probability, can be introduced to combine the two path loss models and we have

$$l_{k,m} = p_{\text{LOS}}(d_{k,m})\text{PL}_{\text{LOS}} + (1 - p_{\text{LOS}}(d_{k,m}))\,\text{PL}_{\text{NLOS}}. \tag{3.31}$$

  Here, the LOS/NLOS path loss models and LOS probability may be chosen according to the preciously mentioned models.

CHAPTER 4

Integrated Access and Backhaul Networks

The dense deployment of mmWave BSs can significantly improve the coverage and throughput of 5G networks. However, one of the biggest challenges is to provide backhaul links to every BS. It may be impractical to install fiber links for backhauling as the cost is high and asking for permission can be difficult. Wireless backhaul is an alternative solution when fiber installation is not feasible or economically viable. With this background, 3GPP has proposed IAB, as a specially kind of wireless backhaul where the same node performs both the access and the backhaul communications. In an IAB network, BSs with fixed backhaul links can forward backhaul data for BSs without fixed, e.g., wired, backhaul links using the same frequency, hardware, and protocols as access networks. The performance of IAB networks has received great attention recently [56], [59], [116] and it is shown that, with a proper deployment, IAB networks are robust against blockage, rain and foliage effects. Since the backhaul transmission may share the same resources as the access transmission, how to schedule the channel usage and optimize resource allocation is important for the IAB networks to achieve high throughput.

In this chapter, we introduce the IAB concept, in particular, we present the network structure in Sec. 4.1 and the IAB scheduling optimization problems in CoMP in Sec. 4.2.

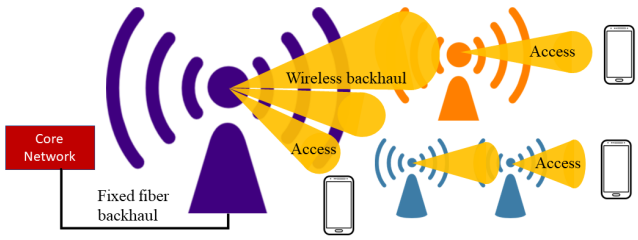

Figure 4.1: An example of IAB network structure.

4.1 IAB in mmWave Networks

Due to the fact that mmWave BSs have a shorter transmission range and higher density than macro BSs, IAB can provide an efficient way of providing the backhaul links to mmWave BSs. In addition, by using hybrid beamforming with cell-free massive MIMO, where antennas are distributed among several access points, backhaul and access transmissions can be optimized to improve the end-to-end user rate [117].

IAB can provide wireless backhaul to BSs in both indoor and outdoor environments, relay nodes and fixed access networks. The key features to be supported by the first release of 3GPP IAB network for NR backhauling (Rel-16) are

- Multi-hop backhauling: to enable flexible range extension.
- QoS differentiation and enforcement: to ensure that the 5G QoS of bearers is fulfilled even in a multi-hop setting.
- Support for network topology adaptation and redundant connectivity: for optimal backhaul performance and fast adaptation to backhaul radio link overloads and failures.
- In-band and out-of-band relaying: the use of the same or different carrier frequency for the access (i.e. link to UEs) and backhaul links (i.e. link to other network nodes) of the IAB node, respectively.
- Support for legacy terminals: the deployment of IAB nodes should be transparent to UEs (i.e. no new UE features/standardization required).

Figure 4.1 shows an example of an IAB network where the BS with the fixed, e.g., fiber, backhaul link can forward wireless backhaul data for the BSs without fixed backhaul links in the same frequency as the access links. By operating the wireless backhaul and user access links within the same frequency band, the spectral

efficiency is maximized through coordinated scheduling and optimized resource allocation. Furthermore, they can function as multi-hop nodes, cascading backhaul data to more distant base stations deeper in the network topology. Leveraging spatial multiplexing and advanced beamforming, an IAB-node can simultaneously service access traffic to UEs and transport backhaul traffic to neighboring BSs, significantly multiplying network capacity without requiring additional spectrum.

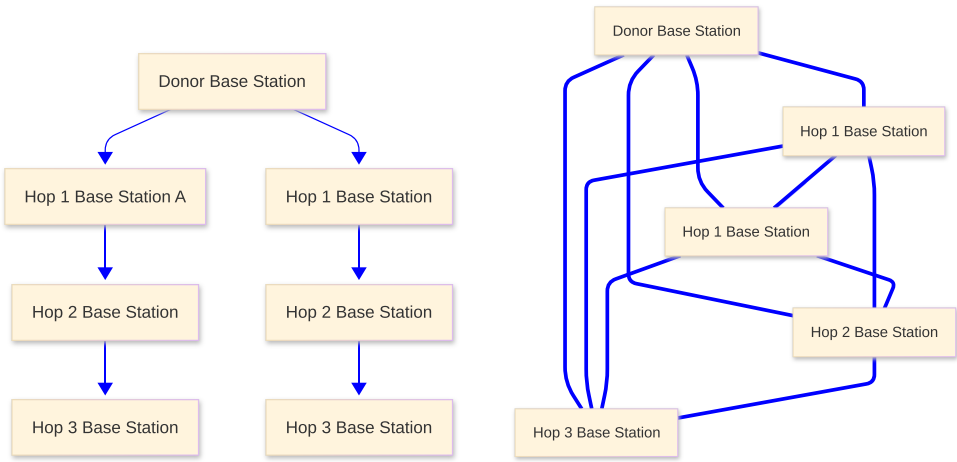

(a) Hierarchical Architecture. **(b)** Mesh Architecture.

Figure 4.2: Examples of IAB network topology.

Depending on the type of backhaul links, BSs with fixed backhaul links that transmit backhaul data for other BSs are referred to as donor nodes, the rest of BSs using wireless backhaul links are called IAB nodes. As shown in Fig. 4.2, depending on the network topology, it is possible that IAB nodes which are near the donor act as relays and further transmit backhaul data with multiple hops for IAB nodes which are far away. IAB network topology is hierarchical if backhaul transmissions between IAB nodes with the same number of hops to the donor are not allowed, while meshed IAB networks allow transmissions between any IAB nodes.

One of the main drawbacks of IAB is the large communication overhead for multi-hop networks and it may lead to complex IAB nodes scheduling. There is also a routing problem since the donor IAB nodes need to configure a route to the destination node and separate routing rules may be considered for the DL and UL direction. IAB network deployment also needs to be carefully designed. It has been shown that, considering geographical and inter-node distance constraints, proper network planning can boost the coverage of the IAB networks significantly [118]. In addition, topology adaptation for IAB networks may be needed due to the blockage effects. IAB topology adaptation can be triggered by the integration of a new IAB node to

the topology, detachment/release of an IAB node from the topology, detection of backhaul link overload, deterioration of backhaul link quality, link failure, or other events.

Due to the half-duplex constraint, there is a need for strict time-domain separation for the IAB-node operational mode in order to account for different levels of interference [119]. IAB node time-domain resources may be configured as Downlink, Uplink, or Flexible, indicating the possible transmission direction of a given resource. Due to the directional transmissions, the backhaul link interference should be limited by carefully designing the TDD frame formats and optimizing the backhaul and access slot allocations based on different QoS requirements. It is shown that algorithms that update the access users according to the backhaul scheduling results can greatly improve the system throughput [120].

How to maximize the throughput and the energy efficiency of wireless backhaul links has received less attention. The scheduling processes such as Round Robin is impractical. When multi-hop transmissions should be used is an important issue to study.

4.2 IAB Throughput Optimization

Due to the fact that IAB networks consist of multi-hop transmissions and mmWave links are sensitive to blockages, the scheduling problem which optimally allocates time resources for multi-hop transmissions is important to achieve high throughput and ensure minimum QoS requirements. Therefore, scheduling and allocating time resources for every access and backhaul link is an important aspect of IAB throughput optimization.

4.2.1 System Model

The common assumptions to be made in IAB networks are (i) the resources are measured in discrete units of time slots or packets and (ii) a flow has to be scheduled sequentially, i.e., a hop closer to the source should be scheduled earlier than a hop farther away. Graphs can be used to represent the network topology where the IAB nodes or users that receive data from doner IAB node m are treated as the child nodes of doner IAB node m, and the maximum number of child nodes per doner IAB node is denoted by C. The network expands from the IAB nodes with fixed backhaul links in a tree structure such that there are $R+K$ links in the network. Here R denotes the number of IAB nodes with fixed backhaul links and K denotes the number of IAB nodes with wireless backhaul. The IAB nodes can receive backhauling data from the doner IAB nodes, and each IAB node maintains a number of access links in order to serve the user nodes.

We assume that the IAB nodes can only transmit or receive, i.e., not simulta-

neously, in a given time slot, and the doner IAB nodes transmit to their serving users and associated IAB nodes in a time-division multiple access (TDMA) manner. Hence, only one of the links connected to an IAB node can be active, and the active links can not share a common doner IAB node at a given time. Furthermore, we divide each frame into a number of time slots with variable length t_i. Assuming a time frame where $\sum_{i=1}^{N} t_i = T$, N is the number of time slots in the frame and T is the frame duration. The number of transmitted bits between nodes m and k can then be defined as $\gamma_{m,k} = \sum_{i=1}^{N} t_i c_{m,k}$ where $c_{m,k}$ denotes the capacity of the link between node m and node k. If the link $m \to k$ is not active in time slot t_i, we assume $c_{m,k} = 0$. Hence, the total throughput delivered to a node k is given by

$$r_k = \frac{\sum_{m \in B_k} \gamma_{m,k} - \sum_{n \in A_k} \gamma_{k,n}}{T}, \tag{4.1}$$

$$= \frac{\sum_{i=1}^{N} t_i \left(\sum_{m \in B_k} c_{m,k} - \sum_{n \in A_k} c_{k,n} \right)}{T} \tag{4.2}$$

where B_k is the set of doner IAB nodes to node (either IAB node or user) k and A_k is the set of nodes to which node k transmits data. Denote $\mathbf{t} = [t_1, \cdots, t_N]$ and $\mathbf{C} = [\mathbf{c}_1, \cdots, \mathbf{c}_i, \cdots, \mathbf{c}_N]$ as the capacity matrix where the elements in $\mathbf{c}_i$ are the aggregated rates of each node based on a given link activation pattern in time slot t_i, i.e., $\mathbf{c}_i[k] = \sum_{m \in B_k} c_{m,k} - \sum_{n \in A_k} c_{k,n}, \forall k$.

In general, assuming node k is required to achieve a minimum throughput θ_k. Thus, the objective is to maximize the minimum throughput of the nodes in the access network subject to the time resource constraint. Such an optimization guarantees better fairness in the network, at the cost of losing the peak access rate for the users with good link quality. Let $\mathcal{S}$ be a schedule where in each time slot a certain set of links are active and assume a normalized frame where $T = 1s$, the problem can be formulated as

$$\mathcal{P}_6 : \max_{\mathbf{t}, \mathcal{S}} \quad \theta \tag{4.3}$$

$$\text{s.t.} \quad \mathbf{C}\mathbf{t} \geq \theta \mathbf{w}_\theta \tag{4.4}$$

$$\mathbf{1}^T \mathbf{t} = 1 \tag{4.5}$$

$$\mathbf{t} \geq \mathbf{0}, \tag{4.6}$$

where θ is the minimum throughput, (4.4) is the minimum throughput constraint for all nodes, $\mathbf{w}_\theta$ contains the weights for achieving different throughput and providing larger throughput for users with higher data demand, (4.5) is the unit frame length constraint and (4.6) is the non-negative constraint for time slot length. Here, we are interested in maximizing the minimum throughput to the users. To that end, for IAB nodes we can simply set the weights to be 0 so that the BSs are treated as gateways to provide throughput to the users.

The above optimization problem can be solved by linear programming. In Paper B, i.e., [67], we propose a revised simplex algorithm that can solve $\mathcal{P}_6$ and it gives the optimal time scheduling schemes which determines the number of active links in each time slot. We also evaluate the effect of different parameters such as blockage, antenna gain and network density on the system performance, and compare the results of IAB networks with those achieved in the cases with traditional non-IAB networks. However, further study is needed to address the induced delay due to control signaling and investigate the impact of mobility and network reconfiguration on the network performance.

CHAPTER 5

Conclusions and Future works

5.1 Contributions

The purpose of this thesis is to provide analytical performance analysis of heterogeneous networks as well as investigate resource allocations in mmWave networks using beamforming. Performance metrics including coverage probability and ASE are derived in closed-form equations in PPP-based networks, and the analysis in mmWave networks highlights the energy-efficient hybrid precoding algorithms and the high throughput in IAB networks. The following subsections summarize the contributions in heterogeneous networks and mmWave networks.

5.1.1 Resource Allocation in mmWave Networks

In a multi-cell multi-user network, the joint optimization of the BSs power consumption is studied to minimize the sum power consumption of the BSs subject to per-user spectral efficiency constraints as well as the per BS peak power constraints. The hybrid beamforming architectures are exploited to reduce the hardware power consumption and complexity and efficient precoding algorithms are given for achieving BS joint transmissions. In IAB networks, a scheduling optimization of access and backhaul links and the effect of the network topology and antenna parameters are studied in order to maximize the minimum access networks' throughput.

Paper A: "Hybrid Precoding in Cooperative Millimeter Wave Networks" This paper studies hybrid beamforming algorithms that enable joint transmissions

in a cooperative multi-cell multi-user mmWave network, for both FHP and PHP, for single-carrier and OFDM systems.The proposed algorithm allows to minimize the total RF and hardware power consumption under per-user target spectral efficiency constraint and per-BS maximum RF transmit power constraint, and finds the optimal user associations and the BS silence strategy. By allowing joint transmissions from multiple BSs to each user, we first show that the joint analog and digital precoding problems can be decoupled into independent equal-gain transmission problems and relaxed convex semidefinite programs. Then, we analyze the Lagrangian dual problem of the convex digital precoder optimization problem, which gives the conditions for the optimal user association strategy that minimizes the sum power consumption of the network. Next, based on the convex envelope of the objective function of the hybrid beamforming algorithm, we propose a sub-optimal hybrid precoding algorithm in terms of the silence strategy with low complexity. Simulations on the power consumption verifies that the FHP achieves similar RF transmit power compared to the FDP, and the hardware power consumption has a large impact on the sum power consumption of the hybrid precoding architectures. Furthermore, cooperative transmissions are shown to achieve increased energy efficiency, reduced sum power consumption of the network, lower infeasibility probability, and lower RF transmit power variations.

Contributions: Chao Fang proposed the hybrid beamforming algorithms, derived most of the mathematical analysis, developed most of the simulation software, verified the performance with simulations and wrote the paper. Behrooz Makki suggested related literature, contributed to the proposal of the system model and the analysis of the simulation results, and proofread the paper. Jingya Li provided the baseline code for convex optimization and helped in deriving the joint transmission rate. Tommy Svensson suggested related literature, contributed to the problem formulation, system model, the planning and analysis of the simulation results, and proofread the paper.

Paper B: "Joint Scheduling and Throughput Maximization in Self-backhauled MillimeterWave Cellular Networks"

In Paper B, we develop a minimum throughput maximization algorithm for mmWave IAB networks. Our model considers the path loss difference due to blockages and the antenna array gains depending on if angle of departure (AODs) or angle of arrival (AOAs) are within the main lobe. Based on the considered channel model, we maximize the minimum throughput of each access link based on the revised simplex method. The simulation results show that the achievable minimum throughput of IAB networks outperforms that of the macro-only networks for a broad range of power levels and IAB networks can provide better throughput in denser environments. Moreover, we show that the achievable minimum throughput increases by

densifying the network with IAB nodes, reducing the number of backhaul hops, increasing the transmit antenna main lobe gain or reducing the main lobe beam width.

Contributions: Chao Fang proposed the minimum throughput maximization algorithm, derived the mathematical analysis, developed the simulation software, verified the performance with simulations and wrote the paper. Behrooz Makki suggested related literature, contributed to the proposal of the system model and the analysis of the simulation results, and proofread the paper. Charitha Madapatha Madapathage Dons commented on the problem formulation and proofread the paper. Tommy Svensson suggested related literature, contributed to the problem formulation, system model, the planning and analysis of the simulation results, and proofread the paper.

5.1.2 Coverage Analysis in Heterogeneous Networks

Using stochastic geometry, key network metrics including coverage probability, successful transmission probability and area spectral efficiency can be expressed in closed-form equations, which allows for efficient and accurate network parameters design of BS density and the number of antennas.

Paper C: "Equal Gain Combining in Poisson Networks with Spatially Correlated Interference Signals"
The effect of spatial correlation on the successful reception probability for an EGC receiver is studied in this paper. Analytical expressions and approximations of the successful reception probability are derived for two-antenna and more than two antennas, respectively. Also, we derive a further simplified successful reception probability and find the optimal density maximizing the ASE. The results demonstrate the substantial effect of the spatial correlation on multi-antenna networks and the potential of diversity combiners to increase the successful reception probability in unstructured networks.

Contributions: Chao Fang derived the mathematical equations, developed the simulation software, verified the performance with simulations and wrote the paper. Behrooz Makki suggested related literature, contributed to the proposal of the system model and the analysis of the simulation results, and proofread the paper. Xiaodong Xu contributed to the mathematical equations and simulation results through discussions. Tommy Svensson suggested related literature, contributed to the problem formulation, system model, the planning and analysis of the simulation results, and proofread the paper.

Paper D: "Coverage Analysis for Millimeter Wave Uplink Cellular Net-

works with Partial Zero-forcing Receivers"
Paper D analyzes the uplink coverage probability in a mmWave cellular system where users are equipped with single antennas and BSs utilize multi-antenna PZF receivers for useful signal enhancement and interference cancellation. Considering a LOS probability function-based path loss model, the coverage probability is shown to be maximized when using a subset of antennas' degree-of-freedom for useful signal enhancement and using the remaining degrees of freedom for canceling the interference from strongest interferers. Due to the blockage effects and the high attenuation of mmWave signals, the number of strong interferers is small. Thus, most of antennas' degrees of freedom should be used for useful signal enhancement. Particularly, compared to zero-forcing, the PZF scheme is shown to improve the coverage probability significantly.

Contributions: Chao Fang derived most of the mathematical analysis, developed the simulation software, verified the performance with simulations and wrote the paper. Behrooz Makki suggested related literature, contributed to the deriving the analytical results and the analysis of simulation results, and proofread the paper. Tommy Svensson suggested related literature, contributed to the problem formulation, system model, the planning and the analysis of the simulation results, and proofread the paper.

Paper E: "On the Performance of the Poisson-point-process-based Networks with No Channel State Information Feedback"
We study the network performance of cellular networks where BSs locations are modeled by homogeneous PPP. Firstly, we derive the closed-form expression for optimal transmission rate maximizing the per-user throughput and find that maximum per-user throughput increases with BS density and transmit power as a result of increased coverage probability. However, the optimal rate is a constant and does not dependent on BS density or transmit power. For a special case of path loss exponent equal to 4, we derive the necessary condition for a positive diversity gain and a tight approximation for the effective density indicating the current BSs with transmitting SINR larger than a threshold. The results show that the BS density needs to decrease with increasing transmit power at least polynomially in order to have a positive diversity gain, and the effective density depends on the transmission rate, transmit SNR and coverage probability. For other path loss exponents, we give approximation of the coverage probability from which we gain insights that larger path loss exponents give better coverage probability due to reduced interference power.

Contributions: Chao Fang derived most of the mathematical equations, developed the simulation software, verified the performance with simulations and wrote the paper. Behrooz Makki suggested related literature, proposed the problem, contributed

to the deriving of the analytical results and the analysis of the simulation results and proofread the paper. Tommy Svensson suggested related literature, contributed to the problem formulation, system model and the planning and analysis of the simulation results, and proofread the paper.

5.1.3 Related contributions

mmWave systems are able to achieve high data rate transmissions with large spectrum and carrier bandwidth. However, due to the high operating frequencies, hardware design can be more challenging than lower-band systems. One particular issue is that phase noise of real oscillators often increases with operating frequencies, resulting in higher inter-carrier interference (ICI) for OFDM systems. In Paper I, i.e.[121], the impact of oscillator phase noise is analysed in a MIMO OFDM system. For the common oscillator case, where all transmit or receiver antennas share the same oscillator, the phase noise at the transmitter and the receiver is shown to influence the signal error vector magnitude (EVM) equally. For the independent oscillator case where each antenna has a dedicated oscillator, the phase noise at the transmitter is shown to have a larger effect on EVM than that of the receiver side. It is also found that ICI caused by the common oscillator can be compensated for by advanced phase noise mitigation schemes, resulting in better EVM performance than that in the independent oscillator case.

As the densification of networks continues, IAB is a cost-efficient way to alleviate the high cost of deploying fiber links to each BS. To achieve high spectral efficiency at the same time, IAB networks require a comprehensive standardization as well as careful network planning. The 3GPP standardization progress for IAB mentioned in Paper F, i.e. [59], provides an overview of IAB architecture in the Rel-16 and Rel-17. By modelling BSs' locations with stochastic geometry, several network models including IAB, hybrid IAB/fiber-connected, and fiber-connected networks are compared in terms of coverage probability and the effect of rain, blocking and foliage on coverage probability is simulated. The results demonstrate that IAB is a flexible method for network densification.

Heterogeneous networks consisting of BSs with different transmit power and coverage area has become one important aspect of 5G. To model the network performance with high accuracy and low complexity, stochastic geometry has been used to provide useful insights of many network parameters including network density, transmit power, ect. on the coverage provability, energy- and spectral-effciency. In Paper K, i.e. [60], we analyze the effect of HARQ schemes on coverage probability and per-user throughput in heterogeneous networks. In Paper J, i.e. [122], the effect of PA efficiency on the outage probability, per-user throughput and ASE is analysed in PPP-based networks with different codeword lengths. Finally, delay-sensitive ASE, which is the ratio between the achievable throughput and the affected area, is op-

timized in terms of optimal rate and power allocation in both point-to-point and PPP-based networks.

5.2 Future Work

In this thesis, we have studied hybrid precoding in multi-BS multi-user mmWave systems and have demonstrated its high energy-efficiency and low hardware complexity. We consider the FHP and PHP architectures where each antenna is connected to all of the RF chains or a fixed subsection of the RF chains through PSs. We have seen that PHP requires more transmit power to achieve the same target spectral efficiency as that of FHP, due to the HW limitations. A more flexible design would be optimizing the inter-connections between RF chains and antennas in PHP so that the spectral efficiency of PHP can approach that of FHP or FDP with reduced HW power consumption and complexity.

We have so far used a simplified system model by omitting many of the HW impairments. One of such impairments that is worth further exploration is to consider non-ideal PSs in hybrid beamforming architectures. Phase offsets caused by practical PSs can result in incorrect beam directions and loss of array gain. Efficient algorithms that can estimate and compensate for the phase offsets could provide significant performance enhancement for hybrid beamforming.

Distributed MIMO (D-MIMO) or cell-free (CF) MIMO is an interesting topic to explore for 6G [107], [123], [124]. By distributing a large number of antenna elements or access points (APs) with multiple antennas across the network to jointly serve users, inter-cell interference can be reduced by exploiting macro diversity. To achieve the full potential of D-MIMO, precoding and power control of all APs need to be centrally computed, which requires fronthaul networks that exchange control signals between APs and central processing units. Therefore, it is an important topic to study to the trade-off optimization between fronthaul rate and access rate. Another important topic is to study AP selection algorithms for achieving high energy and spectrum efficiency considering load balance and QoS constraints.

5.3 Appendix

Consider a network where transmitters are modelled by a homogeneous PPP with density λ. According to Slivnyak's theorem, adding a point at a given location does not change the distribution of the PPP, thus we assume a receiver is dropped at the origin of a 2D plane and attempts to decode a message from a transmitter x_s at distance $||x_s|| = d$. All other transmitters are treated as interfering sources. The receiver is assumed to be equipped with N antennas and perform diversity combining to enhance the received SINR. Denoting the location of each interfering transmitter by $x \in \Phi$ and the transmit power of all transmitters by P, with independent and

identically distributed (IID) Rayleigh fading and a path loss on all signal paths, the received random complex signal on the i-th antenna can be expressed as

$$s_i = \sqrt{P} d^{-\alpha/2} g_i e^{j\theta_i} m_i + \sum_{x \in \Phi} \sqrt{P} ||x||^{-\alpha/2} g_{i,x} e^{j\theta_{i,x}} m_{i,x} + n_0. \tag{5.1}$$

Here, $||x||$ is the distance from each interfering BS to the considered user, g_i and $g_{i,x}$ are IID Rayleigh random variables with the scale parameter $\sqrt{1/2}$, $\alpha > 2$ is the path loss exponent, n_0 is the additive noise amplitude. Also, $\theta_i, \theta_{i,x}$ are the phase associated with each signal path, m_i and $m_{i,x}$ are the power-normalised transmitted symbols from the desired transmitter and the interfering transmitters, respectively.

The receiver receives multiple copies of the useful signal and interference signals from other transmitters. Received signals are first weighted by a complex number w_i and then summed to form the output signal. The phase of the weight θ_i is chosen to co-phase the useful signals on each antenna, the amplitude of the weight is chosen differently based on the type of combining. After co-phasing, the useful signals can add up coherently, however the interference signals are not co-phased and are added incoherently.

5.3.1 Outage Probability for SSC with Two Receive Antennas

Here, we analyze the outage probability for SSC with two receive antennas. Compared to MRC, EGC and SC, SSC is the least complicated as the SIR condition is monitored only on one antenna, thus only one detector is needed. Because of the simplicity of the SSC scheme, it is interesting to assess the outage probability for two-antenna SSC and study the effect of interference correlation on it.

Let θ_{SSC} denote the switching threshold. The cumulative distribution function (CDF) of SIR at a receiver performing SSC with two receive antennas to decode the information from a transmitter at distance d is given by

$$\mathbb{P}\left(\text{SIR}_{\text{SSC}} < T\right) = \begin{cases} 1 - p(T) - p(\theta_{\text{SSC}}) + q(T, \theta_{\text{SSC}}), & T < \theta_{\text{SSC}} \\ 1 - 2p(T) + q(T, \theta_{\text{SSC}}), & T \geq \theta_{\text{SSC}} \end{cases} \tag{5.2}$$

$$p(x) = e^{-\lambda \pi d^2 \Gamma(1+\delta)\Gamma(1-\delta) x^{\delta}} \tag{5.3}$$

$$q(x, y) = e^{-\lambda \pi d^2 B(\delta+1, 1-\delta) x^{\delta} \left(1 + \delta \ {}_2F_1(1, \delta+1; 2; 1-\frac{x}{y})\right)}, \tag{5.4}$$

with ${}_2F_1(a, b; c; d)$ and $B(x, y)$ denoting Hypergeometric function and Beta function, respectively, and $\delta = 2/\alpha$.

Proof. The CDF of the SIR for the SSC is given by

$$\mathbb{P}\left(\mathrm{SIR}_{\mathrm{SSC}} < T\right) = \begin{cases} \mathbb{P}\left(\mathrm{SIR}_1 < \theta_{\mathrm{SSC}} \text{ and } \mathrm{SIR}_2 < T\right), & \theta_{\mathrm{SSC}} < T \\ \mathbb{P}\Bigg((\theta_{\mathrm{SSC}} < \mathrm{SIR}_1 < T) \\ \quad \text{or } (\mathrm{SIR}_1 < \theta_{\mathrm{SSC}} \text{ and } \mathrm{SIR}_2 < T) \Bigg), & \theta_{\mathrm{SSC}} \geq T, \end{cases} \tag{5.5}$$

where SIR_1 and SIR_2 refer to the SIR on each antennas which is given by the SIR on each antenna before weighting, and is given by

$$\mathrm{SIR}_i = \frac{d^{-\alpha} g_i^2}{\sum_{x \in \Phi} ||x||^{-\alpha} g_{i,x}^2}. \tag{5.6}$$

Here, each of $g_i^2, g_{i,x}^2$ follows an exponential distribution with unit mean.

We first derive the CDF for $\theta_{\mathrm{SSC}} < T$. Since the interference on two antennas are correlated, the first joint probability in (5.5) can be expressed as

$$\begin{aligned} &\mathbb{P}\left(\mathrm{SIR}_1 < \theta_{\mathrm{SSC}} \text{ and } \mathrm{SIR}_2 < T\right) \\ &= 1 - \mathbb{P}(\mathrm{SIR}_1 > \theta_{\mathrm{SSC}} \text{ or } \mathrm{SIR}_2 > T) \\ &= 1 - \mathbb{P}(\mathrm{SIR}_1 > \theta_{\mathrm{SSC}}) - \mathbb{P}(\mathrm{SIR}_2 > T) + \\ &\quad \mathbb{P}(\mathrm{SIR}_1 > \theta_{\mathrm{SSC}}, \mathrm{SIR}_2 > T), \end{aligned} \tag{5.7}$$

where $\mathbb{P}(\mathrm{SIR} > x)$ is the CCDF of the SIR for single antenna transmission and is given by

$$\mathbb{P}(\mathrm{SIR} > x) = e^{-\lambda \pi d^2 \Gamma(1+\delta)\Gamma(1-\delta) x^{\delta}}, \tag{5.8}$$

and

$$\begin{aligned} &\mathbb{P}(\mathrm{SIR}_1 > \theta_{\mathrm{SSC}}, \mathrm{SIR}_2 > T) \\ &= \mathbb{P}(g_1^2 > \theta_{\mathrm{SSC}} d^{\alpha} I_1, g_2^2 > T d^{\alpha} I_2) \\ &= \mathbb{E}_{h,\Phi}\left[\prod_{x \in \Phi} e^{-\theta_{\mathrm{SSC}} d^{\alpha} h_{1,x} ||x||^{-\alpha}} e^{-T d^{\alpha} h_{2,x} ||x||^{-\alpha}} \right] \\ &\overset{(f)}{=} \exp\left(-2\pi\lambda \int_0^{\infty} \left(1 - \frac{y^{\alpha}}{y^{\alpha} + \theta_{\mathrm{SSC}} d^{\alpha}} \times \frac{y^{\alpha}}{y^{\alpha} + T d^{\alpha}} \right) y \, \mathrm{d}y \right) \end{aligned} \tag{5.9}$$

$$\overset{(g)}{=} \exp\left(-\lambda\pi\delta\Big(\int_0^\infty \frac{Td^\alpha z^{\delta-1}}{z+TD^\alpha}\,\mathrm{d}z + \int_0^\infty \frac{\theta_{\mathrm{SSC}} d^\alpha z^\delta}{(z+\theta_{\mathrm{SSC}}d^\alpha)(z+Td^\alpha)}\,\mathrm{d}z\Big)\right)$$
$$\overset{(h)}{=} \exp\left(-\lambda\pi d^2 B(\delta+1,1-\delta)T^\delta\left(1+\delta_2 F_1\left(1,\delta+1;2;1-\frac{T}{\theta_{\mathrm{SSC}}}\right)\right)\right), \quad (5.10)$$

where (f) follows from the IID fading coefficients $h_{1,x}, h_{2,x}$ and the probability generating function for the PPP, (g) is from variable transforms $y^\alpha \to z, \delta \to 2/\alpha$. Also, (h) uses the integral calculation that

$$\int_0^\infty \frac{\theta_{\mathrm{SSC}} d^\alpha z^\delta}{(z+Td^\alpha)(z+\theta_{\mathrm{SSC}}d^\alpha)}\,\mathrm{d}z = T^\delta d^2 B(\delta+1,1-\delta)_2F_1\left(1,\delta+1;2,1-\frac{T}{\theta_{\mathrm{SSC}}}\right), \quad (5.11)$$

and

$$\int_0^\infty \frac{Td^\alpha z^{\delta-1}}{z+Td^\alpha}\,\mathrm{d}z = T^\delta d^2 B(1-\delta,\delta). \quad (5.12)$$

Plugging (5.8) and (5.10) into (5.7), we have the outage probability for the SSC scheme.

■

For $\theta_{\mathrm{SSC}} \geq T$,

$$\begin{aligned}
&\mathbb{P}\Big((\theta_{\mathrm{SSC}} < \mathrm{SIR}_1 < T) \text{ or } (\mathrm{SIR}_1 < \theta_{\mathrm{SSC}} \text{ and } \mathrm{SIR}_2 < T)\Big) \\
&= \mathbb{P}\left(\theta_{\mathrm{SSC}} < \mathrm{SIR}_1 < T\right) + \mathbb{P}\left(\mathrm{SIR}_1 < \theta_{\mathrm{SSC}} \text{ and } \mathrm{SIR}_2 < T\right) \\
&= 1 - 2\mathbb{P}(\mathrm{SIR}_2 > T) + \mathbb{P}(\mathrm{SIR}_1 > \theta_{\mathrm{SSC}}, \mathrm{SIR}_2 > T). \quad (5.13)
\end{aligned}$$

Finally, plugging (5.8) and (5.10) into (5.13), we have the outage probability for $\theta_{\mathrm{SSC}} \geq T$. If the interference power on the two receive antennas are uncorrelated, (5.5) is simplified to

$$\mathbb{P}\left(\mathrm{SIR}_{\mathrm{SSC}} < T\right) = \begin{cases} \mathbb{P}(\mathrm{SIR} < \theta_{\mathrm{SSC}})\mathbb{P}(\mathrm{SIR} < T), & T < \theta_{\mathrm{SSC}} \\ \mathbb{P}(\mathrm{SIR} < T) - \mathbb{P}(\mathrm{SIR} < \theta_{\mathrm{SSC}}) + \\ \mathbb{P}(\mathrm{SIR} < \theta_{\mathrm{SSC}})\mathbb{P}(\mathrm{SIR} < T), & T \geq \theta_{\mathrm{SSC}}. \end{cases} \quad (5.14)$$

Plugging in the CDF of the SIR for single antenna transmission as in (5.10), we obtain the CDF of the SIR for the interference-uncorrelated SSC.

Figure 5.1 shows the CDF of the SIR for two-antenna SSC and its comparison with two-antenna SC. We observe that SSC performs worse than SC, except at the point $T = \theta_{\mathrm{SSC}}$ where they have the same performance. Thus by choosing the

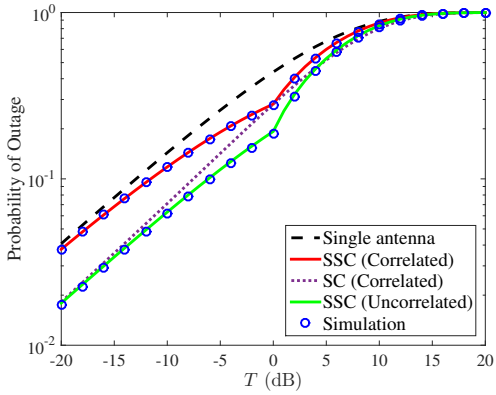

Figure 5.1: Probability of outage for two-antenna SSC as a function of SINR threshold T. SC is considered as the optimal case of SSC in terms of the outage probability. Parameters used to generate the figure are $\lambda = 10^{-3}, d = 10, \alpha = 3.5, \theta_{\text{SSC}} =$ 10 dB.

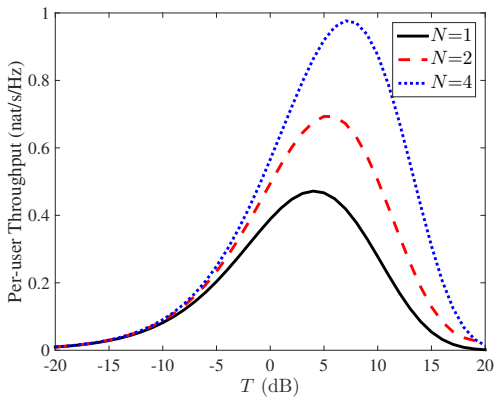

Figure 5.2: Per-user throughput for EGC with different numbers of receive antennas N as a function of SINR threshold T. Parameters used to generate the figure are $\alpha = 3.5, d = 10$.

switch threshold as $\theta_{\text{SSC}} = T$, the outage probability for SSC and SC are the same. Furthermore, Figure 5.1 shows that neglecting the interference correlation gives us underestimated outage probability.

For a given T, the per-user throughput is a monotonic function of the outage probability, hence the previous analysis about the outage probability is also applicable in the per-user throughput. This metric is illustrated in Fig. 5.2. We can see significant per-user throughput improvements by increasing the number of antennas. Interestingly, the figure shows that there exists an optimal transmission rate that maximises the per-user throughput. This is because both the transmission rate and the outage

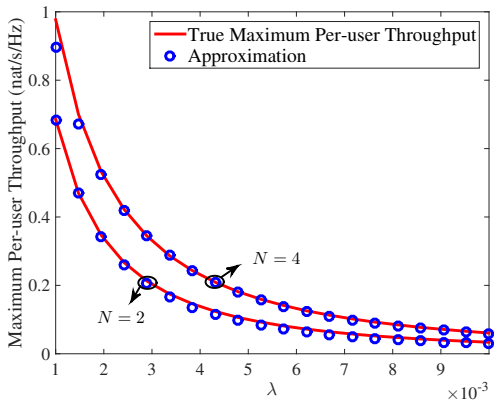

Figure 5.3: Maximum per-user throughput for EGC with different numbers of receive antennas N and BS densities λ. Parameters used to generate the figure are $\alpha = 3.5, d = 10, \hat{T} = -20$ dB.

probability increase with T. Thus there is a trade-off between the outage probability and the transmission rate. In order to find the optimal T, we can derive the optimal rate maximizing the per-user throughput as follows.

The per-user throughput is given by

$$\eta \simeq \log(1+T)\left(1-\left(\frac{T}{\hat{T}}\right)^{\delta} p_o(\hat{T})\right). \tag{5.15}$$

Taking the derivative with respect to T leads to

$$\begin{aligned}\frac{\partial \eta}{\partial T} &\simeq \frac{1-\frac{p_0(\hat{T})}{\hat{T}^{\delta}}T^{\delta}}{1+T} - \log(1+T)\frac{\delta p_o(\hat{T})}{\hat{T}^{\delta}}T^{\delta-1} \\ &\simeq 1 - \frac{(\delta+1)p_o(\hat{T})}{\hat{T}^{\delta}}T^{\delta}, \quad T \to 0. \end{aligned} \tag{5.16}$$

Setting (5.16) to 0, the optimal T maximising the per-user throughput is given by

$$T_{max} \simeq \left(\frac{\hat{T}^{\delta}}{(1+\delta)p_0(\hat{T})}\right)^{\frac{1}{\delta}}. \tag{5.17}$$

Figure 5.3 illustrates the maximum per-user throughput for different values of the transmitter density. The red solid-line curves give the maximum per-user throughput found by numerical search and the blue circles are obtained by using T_{max} given in (5.17). It shows that the simple approximation in (5.17) well matches the true maximum per-user throughput. Also, we notice that as λ increases, the maximum

per-user throughput decreases and the relative outage probability improvements between the cases with different antennas become smaller. This is because, conditioned on fixed distance to the desired transmitter, an increase in the transmitter density leads to higher received interference power. Therefore, adding up noisy received signals lowers the gain from increasing antennas. However, a higher network density allows more users to be served and results in higher overall network throughput.

References

[1] Cisco, "Cisco annual internet report(2018–2023)," White paper, 2020.

[2] A. Zanella, N. Bui, A. Castellani, L. Vangelista, and M. Zorzi, "Internet of things for smart cities," *IEEE Internet Things J.*, vol. 1, no. 1, pp. 22–32, Feb. 2014.

[3] N. Rajatheva, I. Atzeni, S. Bicais, *et al.*, *Scoring the terabit/s goal:broadband connectivity in 6G*, arXiv:2008.07220, 2021.

[4] *Ericsson mobility report*, Ericsson, Nov. 2025.

[5] ITU-R, "Minimum requirements related to technical performance for IMT-2020 radio interface(s)," Tech. Rep., 2016.

[6] M. Shafi, A. F. Molisch, P. J. Smith, *et al.*, "5G: A tutorial overview of standards, trials, challenges, deployment, and practice," *IEEE J. Sel. Areas Commun.*, vol. 35, no. 6, pp. 1201–1221, 2017.

[7] T. S. Rappaport, S. Sun, R. Mayzus, *et al.*, "Millimeter wave mobile communications for 5G cellular: It will work!" *IEEE Access*, vol. 1, pp. 335–349, 2013, ISSN: 2169-3536.

[8] A. Osseiran, J. F. Monserrat, and P. Marsch, *5G Mobile and Wireless Communications Technology*. Cambridge University Press, 2016.

[9] J. G. Andrews, S. Buzzi, W. Choi, *et al.*, "What will 5G be?" *IEEE J. Sel. Areas Commun.*, vol. 32, no. 6, pp. 1065–1082, Jun. 2014, ISSN: 0733-8716.

[10] J. G. Andrews, H. Claussen, M. Dohler, S. Rangan, and M. C. Reed, "Femtocells: Past, present, and future," *IEEE J. Sel. Areas Commun.*, vol. 30, no. 3, pp. 497–508, Apr. 2012, ISSN: 0733-8716.

[11] M. Kamel, W. Hamouda, and A. Youssef, "Ultra-dense networks: A survey," *IEEE Communications Surveys Tutorials*, vol. 18, no. 4, pp. 2522–2545, 2016, ISSN: 1553-877X.

[12] H. S. Dhillon, R. K. Ganti, F. Baccelli, and J. G. Andrews, "Modeling and analysis of K-tier downlink heterogeneous cellular networks," *IEEE J. Sel. Areas Commun.*, vol. 30, no. 3, pp. 550–560, Apr. 2012, ISSN: 0733-8716.

[13] J. G. Andrews, F. Baccelli, and R. K. Ganti, "A tractable approach to coverage and rate in cellular networks," *IEEE Trans. Commun.*, vol. 59, no. 11, pp. 3122–3134, Dec. 2011, ISSN: 0090-6778.

[14] A. AlAmmouri, J. G. Andrews, and F. Baccelli, "A unified asymptotic analysis of area spectral efficiency in ultradense cellular networks," *IEEE Trans. Inf. Theory*, vol. 65, no. 2, pp. 1236–1248, 2019.

[15] M. Haenggi, J. G. Andrews, F. Baccelli, O. Dousse, and M. Franceschetti, "Stochastic geometry and random graphs for the analysis and design of wireless networks," *IEEE J. Sel. Areas Commun.*, vol. 27, no. 7, pp. 1029–1046, 2009.

[16] T. Bai and R. W. Heath, "Coverage and rate analysis for millimeter-wave cellular networks," *IEEE Trans. Wireless Commun.*, vol. 14, no. 2, pp. 1100–1114, Feb. 2015, ISSN: 1536-1276.

[17] M. Di Renzo, "Stochastic geometry modeling and analysis of multi-tier millimeter wave cellular networks," *IEEE Trans. Wireless Commun.*, vol. 14, no. 9, pp. 5038–5057, 2015.

[18] E. Turgut and M. C. Gursoy, "Coverage in heterogeneous downlink millimeter wave cellular networks," *IEEE Trans. Commun.*, vol. 65, no. 10, pp. 4463–4477, 2017.

[19] G. Ghatak, A. De Domenico, and M. Coupechoux, "Coverage analysis and load balancing in HetNets with millimeter wave multi-rat small cells," *IEEE Trans. Wireless Commun.*, vol. 17, no. 5, pp. 3154–3169, 2018.

[20] C. Saha and H. S. Dhillon, "Millimeter wave integrated access and backhaul in 5G: Performance analysis and design insights," *IEEE J. Sel. Areas Commun.*, vol. 37, no. 12, pp. 2669–2684, 2019.

[21] M. Haenggi and R. K. Ganti, *Interference in large wireless networks*. Now Publishers Inc, 2009.

[22] H. Wei, N. Deng, and M. Haenggi, "Performance analysis of inter-cell interference coordination in mm-wave cellular networks," *IEEE Trans. Wireless Commun.*, pp. 1–1, 2021.

[23] C. Fang, B. Makki, X. Xu, and T. Svensson, "Equal gain combining in poisson networks with spatially correlated interference signals," *IEEE Wireless Commun. Lett.*, vol. 5, no. 6, pp. 628–631, 2016.

[24] H. S. Jo, Y. J. Sang, P. Xia, and J. G. Andrews, "Heterogeneous cellular networks with flexible cell association: A comprehensive downlink SINR analysis," *IEEE Trans. Wireless Commun.*, vol. 11, no. 10, pp. 3484–3495, Oct. 2012, ISSN: 1536-1276.

[25] D. Liu, L. Wang, Y. Chen, *et al.*, "User association in 5G networks: A survey and an outlook," *IEEE Communications Surveys Tutorials*, vol. 18, no. 2, pp. 1018–1044, 2016.

[26] H. H. M. Tam, H. D. Tuan, D. T. Ngo, T. Q. Duong, and H. V. Poor, "Joint load balancing and interference management for small-cell heterogeneous networks with limited backhaul capacity," *IEEE Trans. Wireless Commun.*, vol. 16, no. 2, pp. 872–884, 2017.

[27] H. Guo, B. Makki, D.-T. Phan-Huy, E. Dahlman, M.-S. Alouini, and T. Svensson, "Predictor antenna: A technique to boost the performance of moving relays," *IEEE Commun. Mag.*, vol. 59, no. 7, pp. 80–86, 2021.

[28] H. Guo, B. Makki, M.-S. Alouini, and T. Svensson, *High-rate uninterrupted internet-of-vehicle communications in highways: Dynamic blockage avoidance and CSIT acquisition*, 2021.

[29] Q.-V. Pham, F. Fang, V. N. Ha, *et al.*, "A survey of multi-access edge computing in 5G and beyond: Fundamentals, technology integration, and state-of-the-art," *IEEE Access*, vol. 8, pp. 116 974–117 017, 2020.

[30] C. Madapatha, B. Makki, A. Muhammad, E. Dahlman, M.-S. Alouini, and T. Svensson, "On topology optimization and routing in integrated access and backhaul networks: A genetic algorithm-based approach," *IEEE Open Journal of the Communications Society*, vol. 2, pp. 2273–2291, 2021.

[31] C. Madapatha, B. Makki, C. Fang, *et al.*, "On integrated access and backhaul networks: Current status and potentials," *IEEE Open Journal of the Communications Society*, vol. 1, pp. 1374–1389, 2020.

[32] *Measurement results and final mmMAGIC channel models*, Deliverable D2.2, mmMAGIC, May 2017.

[33] S. Sun, T. S. Rappaport, T. A. Thomas, *et al.*, "Investigation of prediction accuracy, sensitivity, and parameter stability of large-scale propagation path loss models for 5G wireless communications," *IEEE Trans. Veh. Technol.*, vol. 65, no. 5, pp. 2843–2860, 2016.

[34] K. Haneda, L. Tian, H. Asplund, *et al.*, "Indoor 5G 3GPP-like channel models for office and shopping mall environments," in *Proc. Int. Conf. Commun Workshops (ICC Workshops)*, Kuala Lumpur, Malaysia, May 2016, pp. 694–699.

[35] T. S. Rappaport, G. R. MacCartney, M. K. Samimi, and S. Sun, "Wideband millimeter-wave propagation measurements and channel models for future wireless communication system design," *IEEE Trans. Commun.*, vol. 63, no. 9, pp. 3029–3056, Sep. 2015, ISSN: 0090-6778.

[36] C.-X. Wang, J. Bian, J. Sun, W. Zhang, and M. Zhang, "A survey of 5G channel measurements and models," *IEEE Communications Surveys Tutorials*, vol. 20, no. 4, pp. 3142–3168, 2018.

[37] J. Huang, C.-X. Wang, H. Chang, J. Sun, and X. Gao, "Multi-frequency multi-scenario millimeter wave MIMO channel measurements and modeling for B5G wireless communication systems," *IEEE J. Sel. Areas Commun.*, vol. 38, no. 9, pp. 2010–2025, 2020.

[38] M. Mezzavilla, M. Zhang, M. Polese, *et al.*, "End-to-end simulation of 5G mmwave networks," *IEEE Communications Surveys Tutorials*, vol. 20, no. 3, pp. 2237–2263, 2018.

[39] *Study on channel model for frequency spectrum above 6GHz*, 3GPP Tech. Rep. 38.900, Jun. 2016.

[40] J. Zhang, E. Björnson, M. Matthaiou, D. W. K. Ng, H. Yang, and D. J. Love, "Prospective multiple antenna technologies for beyond 5G," *IEEE J. Sel. Areas Commun.*, vol. 38, no. 8, pp. 1637–1660, 2020.

[41] O. E. Ayach, S. Rajagopal, S. Abu-Surra, Z. Pi, and R. W. Heath, "Spatially sparse precoding in millimeter wave MIMO systems," *IEEE Trans. Wireless Commun.*, vol. 13, no. 3, pp. 1499–1513, Mar. 2014, ISSN: 1536-1276.

[42] X. Gao, L. Dai, S. Han, C.-L. I, and R. W. Heath, "Energy-efficient hybrid analog and digital precoding for mmwave MIMO systems with large antenna arrays," *IEEE J. Sel. Areas Commun.*, vol. 34, no. 4, pp. 998–1009, Apr. 2016, ISSN: 0733-8716.

[43] J. Mo, A. Alkhateeb, S. Abu-Surra, and R. W. Heath, "Hybrid architectures with few-bit ADC receivers: Achievable rates and energy-rate tradeoffs," *IEEE Trans. Wireless Commun.*, vol. 16, no. 4, pp. 2274–2287, Apr. 2017, ISSN: 1536-1276.

[44] C. Rusu, R. Mèndez-Rial, N. González-Prelcic, and R. W. Heath, "Low complexity hybrid precoding strategies for millimeter wave communication systems," *IEEE Trans. Wireless Commun.*, vol. 15, no. 12, pp. 8380–8393, Dec. 2016, ISSN: 1536-1276.

[45] R. Méndez-Rial, C. Rusu, N. González-Prelcic, A. Alkhateeb, and R. W. Heath, "Hybrid MIMO architectures for millimeter wave communications: Phase shifters or switches?" *IEEE Access*, vol. 4, pp. 247–267, 2016, ISSN: 2169-3536.

[46] X. Gao, O. Edfors, F. Tufvesson, and E. G. Larsson, "Multi-switch for antenna selection in massive MIMO," in *Proc. IEEE Global Telecommun. Conf. (GLOBECOM)*, San Diego, CA, USA, Dec. 2015, pp. 1–6.

[47] Y. Gao, H. Vinck, and T. Kaiser, "Massive MIMO antenna selection: Switching architectures, capacity bounds, and optimal antenna selection algorithms," *IEEE Trans. Signal Process.*, vol. 66, no. 5, pp. 1346–1360, 2018.

[48] S. Jacobsson, G. Durisi, M. Coldrey, and C. Studer, "Linear precoding with low-resolution DACs for massive MU-MIMO-OFDM downlink," *IEEE Trans. Wireless Commun.*, vol. 18, no. 3, pp. 1595–1609, 2019.

[49] M. Sarajlić, L. Liu, and O. Edfors, "When are low resolution adcs energy efficient in massive mimo?" *IEEE Access*, vol. 5, pp. 14 837–14 853, 2017.

[50] O. Orhan, E. Erkip, and S. Rangan, "Low power analog-to-digital conversion in millimeter wave systems: Impact of resolution and bandwidth on performance," in *Proc. Inf. Theory Appl. Workshop (ITA)*, San Diego, CA, USA, Feb. 2015, pp. 191–198.

[51] M. Jafri, S. Srivastava, N. K. D. Venkategowda, A. K. Jagannatham, and L. Hanzo, "Cooperative hybrid transmit beamforming in cell-free mmWave MIMO networks," *IEEE Trans. Veh. Technol.*, vol. 72, no. 5, pp. 6023–6038, 2023.

[52] A. Michaloliakos, W. C. Ao, and K. Psounis, "Joint user-beam selection for hybrid beamforming in asynchronously coordinated multi-cell networks," in *Proc. Inf. Theory Appl. Workshop (ITA)*, La Jolla, CA, USA, Jan. 2016, pp. 1–10.

[53] S. Sun, T. S. Rappaport, M. Shafi, and H. Tataria, "Analytical framework of hybrid beamforming in multi-cell millimeter-wave systems," *IEEE Trans. Wireless Commun.*, vol. 17, no. 11, pp. 7528–7543, Nov. 2018, ISSN: 1536-1276.

[54] A. Alkhateeb, S. Alex, P. Varkey, Y. Li, Q. Qu, and D. Tujkovic, "Deep learning coordinated beamforming for highly-mobile millimeter wave systems," *IEEE Access*, vol. 6, pp. 37 328–37 348, 2018.

[55] C. Fang, B. Makki, J. Li, and T. Svensson, "Hybrid precoding in cooperative millimeter wave networks," *IEEE Trans. Wireless Commun.*, vol. 20, no. 8, pp. 5373–5388, 2021.

[56] X. Ge, H. Cheng, M. Guizani, and T. Han, "5G wireless backhaul networks: Challenges and research advances," *IEEE Network*, vol. 28, no. 6, pp. 6–11, Nov. 2014, ISSN: 0890-8044.

[57] A. Ghosh, N. Mangalvedhe, R. Ratasuk, *et al.*, "Heterogeneous cellular networks: From theory to practice," *IEEE Commun. Mag.*, vol. 50, no. 6, pp. 54–64, Jun. 2012, ISSN: 0163-6804.

[58] *3rd Generation Partnership Project; Technical Specification Group Radio Access Network; Study on Integrated Access and Backhaul; (Release 16)*, 3GPP TR 38.874, Dec. 2018.

[59] C. Madapatha, B. Makki, C. Fang, *et al.*, "On integrated access and backhaul networks: Current status and potentials," *IEEE Open Journal of the Communications Society*, vol. 1, pp. 1374–1389, 2020.

[60] B. Makki, M. Hashemi, L. Bao, and M. Coldrey, "On the performance of FDD and TDD systems in different data traffics: Finite block-length analysis," in *Proc. IEEE Veh. Technol. Conf. (VTC)*, Porto, Portugal, Jun. 2018, pp. 1–5.

[61] O. Teyeb, A. Muhammad, G. Mildh, E. Dahlman, F. Barac, and B. Makki, "Integrated access backhauled networks," in *Proc. IEEE Veh. Technol. Conf. (VTC)*, Honolulu, Hawaii, USA, Sep. 2019, pp. 1–5.

[62] O. P. Adare, H. Babbili, C. Madapatha, B. Makki, and T. Svensson, *Uplink power control in integrated access and backhaul networks*, 2021.

[63] B. Zhuang, D. Guo, E. Wei, and M. L. Honig, "Scalable spectrum allocation and user association in networks with many small cells," *IEEE Trans. Commun.*, vol. 65, no. 7, pp. 2931–2942, 2017.

[64] M. Eslami Rasekh, D. Guo, and U. Madhow, "Joint routing and resource allocation for millimeter wave picocellular backhaul," *IEEE Trans. Wireless Commun.*, vol. 19, no. 2, pp. 783–794, 2020.

[65] M. Polese, M. Giordani, A. Roy, D. Castor, and M. Zorzi, "Distributed path selection strategies for integrated access and backhaul at mmWaves," in *Proc. IEEE Global Telecommun. Conf. (GLOBECOM)*, Waikoloa, HI, USA, Dec. 2018, pp. 1–7.

[66] D. Triantafyllopoulou, K. Kollias, and K. Moessner, "Selfish routing and link scheduling in mmWave backhaul networks," in *Proc. Int. Conf. CommunWorkshops (ICC Workshops)*, Rome, Italy, May 2023, pp. 4200–4205.

[67] C. Fang, C. Madapatha, B. Makki, and T. Svensson, "Joint scheduling and throughput maximization in self-backhauled millimeter wave cellular networks," in *ISWCS*, Berlin, Germany, 2021, pp. 1–6.

[68] H. Tataria, M. Shafi, A. F. Molisch, M. Dohler, H. Sjöland, and F. Tufvesson, "6G wireless systems: Vision, requirements, challenges, insights, and opportunities," *Proc. IEEE*, vol. 109, no. 7, pp. 1166–1199, 2021.

[69] W. Saad, M. Bennis, and M. Chen, "A vision of 6G wireless systems: Applications, trends, technologies, and open research problems," *IEEE Netw.*, vol. 34, no. 3, pp. 134–142, 2020.

[70] M. Giordani, M. Polese, M. Mezzavilla, S. Rangan, and M. Zorzi, "Toward 6G networks: Use cases and technologies," *IEEE Commun. Mag.*, vol. 58, no. 3, pp. 55–61, 2020.

[71] S. Dang, O. Amin, B. Shihada, and M.-S. Alouini, "What should 6G be?" *Nat Electron 3*, pp. 20–29, Jan. 2020.

[72] M. Latva-Aho, "Radio access networkingchallenges towards 2030," in *Proc. 1st Int.Telecommun. Union (ITU-T) Workshop Netw.*, Oct. 2018.

[73] C.-X. Wang, X. You, X. Gao, *et al.*, "On the road to 6G: Visions, requirements, key technologies, and testbeds," *IEEE Communications Surveys & Tutorials*, vol. 25, no. 2, pp. 905–974, 2023.

[74] D. K. Pin Tan, J. He, Y. Li, *et al.*, "Integrated sensing and communication in 6G: Motivations, use cases, requirements, challenges and future directions," in *IEEE International Online Symposium on Joint Communications Sensing (JC&S)*, Dresden, Germany, Feb. 2021, pp. 1–6.

[75] H. S. Dhillon, R. K. Ganti, F. Baccelli, and J. G. Andrews, "Modeling and analysis of k-tier downlink heterogeneous cellular networks," *IEEE J. Sel. Areas Commun.*, vol. 30, no. 3, pp. 550–560, Apr. 2012.

[76] M. Haenggi, *Stochastic geometry for wireless networks*. Cambridge : Cambridge University Press, 2013.

[77] N. Deng and M. Haenggi, "SINR and rate meta distributions for HCNs with joint spectrum allocation and offloading," *IEEE Trans. Commun.*, vol. 67, no. 5, pp. 3709–3722, 2019.

[78] X. Lu, M. Salehi, M. Haenggi, E. Hossain, and H. Jiang, "Stochastic geometry analysis of spatial-temporal performance in wireless networks: A tutorial," *IEEE Communications Surveys Tutorials*, pp. 1–1, 2021.

[79] M. Haenggi, J. G. Andrews, F. Baccelli, O. Dousse, and M. Franceschetti, "Stochastic geometry and random graphs for the analysis and design of wireless networks," *IEEE J. Sel. Areas Commun.*, vol. 27, no. 7, pp. 1029–1046, 2009.

[80] M. Haenggi, *Stochastic Geometry for Wireless Networks*. Cambridge University Press, 2012.

[81] D. Stoyan, W. S. Kendall, and J. Mecke, *Stochastic Geometry and Its Applications, 2nd Edition*. John Wiley and Sons, 1996.

[82] S. M. Azimi-Abarghouyi, B. Makki, M. Haenggi, M. Nasiri-Kenari, and T. Svensson, "Coverage analysis of finite cellular networks: A stochastic geometry approach," in *Iran Workshop on Communication and Information Theory (IWCIT)*, Tehran, Iran, Apr. 2018, pp. 1–5.

[83] S. M. Azimi-Abarghouyi, B. Makki, M. Nasiri-Kenari, and T. Svensson, "Stochastic geometry modeling and analysis of finite millimeter wave wireless networks," *IEEE Trans. Veh. Technol.*, vol. 68, no. 2, pp. 1378–1393, 2019.

[84] S. M. Azimi-Abarghouyi, B. Makki, M. Haenggi, M. Nasiri-Kenari, and T. Svensson, "Stochastic geometry modeling and analysis of single- and multi-cluster wireless networks," *IEEE Trans. Commun.*, vol. 66, no. 10, pp. 4981–4996, Oct. 2018.

[85] M. Haenggi, "On distances in uniformly random networks," *IEEE Trans. Inf. Theory*, vol. 51, no. 10, pp. 3584–3586, 2005.

[86] M. Haenggi, "Diversity loss due to interference correlation," *IEEE Commun. Lett.*, vol. 16, no. 10, pp. 1600–1603, Oct. 2012, ISSN: 1089-7798.

[87] R. Tanbourgi, H. S. Dhillon, J. G. Andrews, and F. K. Jondral, "Effect of spatial interference correlation on the performance of maximum ratio combining," *IEEE Trans. Wireless Commun.*, vol. 13, no. 6, pp. 3307–3316, 2014.

[88] B. Makki and T. Eriksson, "On the performance of MIMO-ARQ systems with channel state information at the receiver," *IEEE Trans. Commun.*, vol. 62, no. 5, pp. 1588–1603, May 2014.

[89] G. Caire and D. Tuninetti, "The throughput of hybrid-ARQ protocols for the Gaussian collision channel," *IEEE Trans. Inf. Theory*, vol. 47, no. 5, pp. 1971–1988, Jul. 2001.

[90] B. Makki and T. Eriksson, "On hybrid ARQ and quantized CSI feedback schemes in quasi-static fading channels," *IEEE Trans. Commun.*, vol. 60, no. 4, pp. 986–997, 2012.

[91] C. Fang, B. Makki, and T. Svensson, "Coverage analysis for millimeter wave uplink cellular networks with partial zero-forcing receivers," in *WiOpt*, Paris, France, 2017, pp. 1–6.

[92] E. Sadeghabadi, S. M. Azimi-Abarghouyi, B. Makki, M. Nasiri-Kenari, and T. Svensson, "Asynchronous downlink massive MIMO networks: A stochastic geometry approach," *IEEE Trans. Wireless Commun.*, vol. 19, no. 1, pp. 579–594, 2020.

[93] K. Ali, H. Elsawy, and M.-S. Alouini, "Meta distribution of downlink non-orthogonal multiple access (NOMA) in poisson networks," *IEEE Wireless Commun. Lett.*, vol. 8, no. 2, pp. 572–575, 2019.

[94] S. Singh, M. N. Kulkarni, A. Ghosh, and J. G. Andrews, "Tractable model for rate in self-backhauled millimeter wave cellular networks," *IEEE J. Sel. Areas Commun.*, vol. 33, no. 10, pp. 2196–2211, 2015.

[95] C. Fang, B. Makki, and T. S. 1, "On the performance of the Poisson-point-process-based networks with no channel state information feedback," *IET Communications*, 2016.

[96] B. Makki, C. Fang, T. Svensson, M. Nasiri-Kenari, and M. Zorzi, "Delay-sensitive area spectral efficiency: A performance metric for delay-constrained green networks," *IEEE Trans. Commun.*, vol. 65, no. 6, pp. 2467–2480, 2017.

[97] *3rd Generation Partnership Project; CoMP operation for LTE physical layer aspects (Release 11)*, 3GPP TR 36.819, Sep. 2013.

[98] H. Dahrouj and W. Yu, "Coordinated beamforming for the multicell multi-antenna wireless system," *IEEE Trans. Wireless Commun.*, vol. 9, no. 5, pp. 1748–1759, May 2010, ISSN: 1536-1276.

[99] E. Björnson and E. Jorswieck, *Optimal Resource Allocation in Coordinated Multi-Cell Systems*. Now Foundations and Trends, 2013.

[100] H. J. Yang, W.-Y. Shin, B. C. Jung, C. Suh, and A. Paulraj, "Opportunistic downlink interference alignment for multi-cell MIMO networks," *IEEE Trans. Wireless Commun.*, vol. 16, no. 3, pp. 1533–1548, 2017.

[101] J. Qiu, K. Xu, X. Xia, Z. Shen, and W. Xie, "Downlink power optimization for cell-free massive MIMO over spatially correlated rayleigh fading channels," *IEEE Access*, vol. 8, pp. 56 214–56 227, 2020.

[102] G. R. MacCartney and T. S. Rappaport, "Millimeter-wave base station diversity for 5G coordinated multipoint (CoMP) applications," *IEEE Trans. Wireless Commun.*, vol. 18, no. 7, pp. 3395–3410, 2019.

[103] D. Gesbert, S. Hanly, H. Huang, S. S. Shitz, O. Simeone, and W. Yu, "Multi-cell MIMO cooperative networks: A new look at interference," *IEEE J. Sel. Areas Commun.*, vol. 28, no. 9, pp. 1380–1408, Dec. 2010, ISSN: 0733-8716.

[104] B. Makki, T. Eriksson, and T. Svensson, "On an HARQ-based coordinated multi-point network using dynamic point selection," *EURASIP Journal on Wireless Communications and Networking*, vol. 2013:209, 2013.

[105] G. Foschini, K. Karakayali, and R. Valenzuela, "Coordinating multiple antenna cellular networks to achieve enormous spectral efficiency," *IEE Proceedings - Communications*, vol. 153, 548–555(7), 4 Aug. 2006.

[106] S. Venkatesan, A. Lozano, and R. Valenzuela, "Network MIMO: Overcoming intercell interference in indoor wireless systems," in *The Forty-First Asilomar Conference on Signals, Systems and Computers, Pacific Grove*, Nov. 2007, pp. 83–87.

[107] S. Elhoushy, M. Ibrahim, and W. Hamouda, "Cell-free massive MIMO: A survey," *IEEE Communications Surveys & Tutorials*, vol. 24, no. 1, pp. 492–523, 2022.

[108] Ö. T. Demir, E. Björnson, and L. Sanguinetti, "Foundations of user-centric cell-free massive MIMO," *Foundations and Trends® in Signal Processing*, vol. 14, no. 3-4, pp. 162–472, 2021.

[109] O. Haliloglu, H. Yu, C. Madapatha, *et al.*, "Distributed MIMO systems for 6G," in *EuCNC/6G Summit, Gothenburg, Sweden*, Jun. 2023, pp. 156–161.

[110] S. P. Boyd and L. Vandenberghe, *Convex Optimization*. Cambridge University Press, 2004.

[111] W. Ni and X. Dong, "Hybrid block diagonalization for massive multiuser MIMO systems," *IEEE Trans. Commun.*, vol. 64, no. 1, pp. 201–211, Jan. 2016, ISSN: 0090-6778.

[112] T. S. Rappaport, Y. Xing, G. R. MacCartney, A. F. Molisch, E. Mellios, and J. Zhang, "Overview of millimeter wave communications for fifth-generation (5G) wireless networks—with a focus on propagation models," *IEEE Trans. Antennas Propag.*, vol. 65, no. 12, pp. 6213–6230, Dec. 2017, ISSN: 0018-926X.

[113] *3rd Generation Partnership Project; Technical Specification Group Radio Access Network; Study on channel model for frequency spectrum above 6 GHz (Release 15)*, TR 38.900, 3GPP, Jun. 2018.

[114] X. Zhang and J. G. Andrews, "Downlink cellular network analysis with multi-slope path loss models," *IEEE Trans. Commun.*, vol. 63, no. 5, pp. 1881–1894, May 2015, ISSN: 0090-6778.

[115] M. K. Samimi, T. S. Rappaport, and G. R. MacCartney, "Probabilistic omnidirectional path loss models for millimeter-wave outdoor communications," *IEEE Wireless Commun. Lett.*, vol. 4, no. 4, pp. 357–360, Aug. 2015, ISSN: 2162-2337.

[116] V. F. Monteiro, F. R. M. Lima, D. C. Moreira, *et al.*, "Paving the way toward mobile IAB: Problems, solutions and challenges," *IEEE Open Journal of the Communications Society*, vol. 3, pp. 2347–2379, Nov. 2022.

[117] A. H. Jazi, S. M. Razavizadeh, and T. Svensson, "Integrated access and backhaul (IAB) in cell-free massive MIMO systems," *IEEE Access*, vol. 11, pp. 71 658–71 667, Jul. 2023.

[118] C. Madapatha, B. Makki, H. Guo, and T. Svensson, "Constrained deployment optimization in integrated access and backhaul networks," in *2023 IEEE WCNC, Glasgow, United Kingdom*, 2023, pp. 1–6.

[119] V. F. Monteiro, F. R. M. Lima, D. C. Moreira, *et al.*, "TDD frame design for interference handling in mobile IAB networks," in *IEEE GLOBECOM, Rio de Janeiro, Brazil*, 2022, pp. 5153–5158.

[120] L. Wang, B. Ai, Y. Niu, *et al.*, "Joint user association and transmission scheduling in integrated mmwave access and terahertz backhaul networks," *IEEE Transactions on Vehicular Technology*, pp. 1–11, Jul. 2023.

[121] X. Chen, C. Fang, Y. Zou, A. Wolfgang, and T. Svensson, "Beamforming MIMO-OFDM systems in the presence of phase noises at millimeter-wave frequencies," in *IEEE Wireless Communications and Networking Conference Workshops (WCNCW),San Francisco, CA, USA*, 2017, pp. 1–6.

[122] C. Fang, B. Makki, Y. Hong, X. Xu, and T. Svensson, "HARQ in poisson point process-based heterogeneous networks," in *IEEE 81st Vehicular Technology Conference (VTC Spring), Glasgow, Scotland*, 2015, pp. 1–5.

[123] M. Ghoraishi, A. Alexiou, T. Cogalan, *et al.*, *Towards Sustainable and Trustworthy 6G: Challenges, Enablers, and Architectural Design*. NOW Publishers, 2023.

[124] J. Zhang, S. Chen, Y. Lin, J. Zheng, B. Ai, and L. Hanzo, "Cell-free massive MIMO: A new next-generation paradigm," *IEEE Access*, vol. 7, pp. 99 878–99 888, 2019.